Electronic Supplementary Material (ESI) for Physical Chemistry Chemical Physics.

On the third-order nonlinear optical responses of *cis* and *trans* stilbene – a quantum chemistry investigation

Komlanvi Sèvi Kaka,[‡] Frédéric Castet,[£] and Benoît Champagne[‡,*]

Electronic supplementary information

TABLE OF CONTENTS

1. Complement on third-order NLO responses and measurements

(i) The degenerate four wave-mixing (DFWM).[S1–4] In this measurement, three beams of frequency ω interact in the material and a fourth beam at the same frequency is produced. Two common geometries can be distinguished: a forward-wave geometry in which all the incident beams are propagating in the same direction and a backward-wave geometry (phase conjugation geometry) which corresponds to the usual experimental configuration of DFWM. In the latter, two beams are counterpropagating (one is a forward pump beam and the second is a backward pump beam) and the third beam (a probe beam) is incident at a small angle with respect to the forward pump beam. The generated wave is proportional to the complex conjugate of the third beam's electric field. In DFWM experiment, electronic, reorientation, and vibrational hyperpolarizabilities as well as thermal effects can be measured and their time response can also be obtained.[S1,5] Going to time resolution of femtoseconds is helpful in separating the various contributions. In this experiment, the quantity that can be extracted from the measurements reads:

$$\gamma_{DFWM}(-\omega;\omega,-\omega,\omega) = \gamma_{//}(-\omega;\omega,-\omega,\omega) = \frac{1}{15}\sum_{ij}^{x,y,z}\left(2\gamma_{iijj} + \gamma_{ijij}\right) \qquad \text{(S1)}$$

(ii) The phase-conjugate interferometry (PCI) experiment also probes $\gamma(-\omega;\omega,-\omega,\omega)$.[S6] In short, the interferometer contains two phase-conjugate mirrors (PCM) based on the DFWM in the retroreflected pump beam configuration. One PCM consists of a cell containing a reference material and the second PCM consists of a cell that contains the organic material to be measured. Using a beam splitter (BS), the two input beams are split into a forward pump (FP) beam and a probe beam. Two retroreflected beams of the FPs by two mirrors serve as backward pump beams (BPs) and recombine together behind the BS. After interaction of the three incident beams with a nonlinear medium placed in each cell/arm, two optical phase-conjugate beams are generated and also combine together at BS. The detail and the optical path of the pump and probe beams can be seen in Figure 1 of Ref. [S6]. Then, the optical path length of one arm of the interferometer is changed with a piezo-electric translator. The two interferograms that arise from the combination of the two retroreflected pump beams and the combination of the two phase-conjugate beams are recorded as a function of the path length. The depth of modulation of the conjugate interferogram is related to the ratio of the amplitude of the third-order susceptibilities of the reference and sample materials. The second hyperpolarizability of organic molecules is thus determined from the measurement performed on a series of the sample solutions at different concentrations. Different nonlinear mechanisms as electronic and orientational effects contribute to the total hyperpolarizabilities in the PCI experiment.

[S6] When the polarizations of the probe and pump are parallel, the second hyperpolarizability quantity reads:

$$\gamma_{PCI}(-\omega;\omega,-\omega,\omega) = \gamma_{//}(-\omega;\omega,-\omega,\omega) = \frac{1}{15}\sum_{ij}^{x,y,z}\left(\gamma_{ijij} + 2\gamma_{ijji}\right) \quad \text{(S2)}$$

Otherwise, when they are perpendicular, the second hyperpolarizability becomes:[7]

$$\gamma_{PCI}(-\omega;\omega,-\omega,\omega) = \gamma_{\perp}(-\omega;\omega,-\omega,\omega) = \frac{1}{30}\sum_{ij}^{x,y,z}\left(3\gamma_{iijj} - \gamma_{ijij}\right) \quad \text{(S3)}$$

(iii) The Kerr experiment. [S8–10] In this technique, the DC field creates a refractive index difference for the parallel and perpendicular polarization and the measured quantity is the so-called molar Kerr constant, given by: [S11]

$$A_K = \frac{N_A}{81\epsilon_0}\left\{\gamma^K(-\omega;\omega,0,0) + \frac{2\mu\beta^K}{3kT} + \frac{3}{10}\left[\frac{\sum_{ij}^{x,y,z}\alpha_{ij}\alpha_{ij} - \alpha\alpha}{kT}\right] + \frac{\mu^2(\alpha_{xx}-\alpha)}{(kT)^2}\right\} \quad \text{(S4)}$$

where, N_A is Avogadro's number, β^K is the dc-Pockels first hyperpolarizability [i.e., $\beta(-\omega;\omega,0)$], $\alpha = \frac{1}{3}\sum_{i}^{x,y,z}\alpha_{ii}$, is the mean polarizability, x denotes the space-fixed direction of the applied DC field, and γ^K is the second hyperpolarizability that is actually measured: [S7,12,13]

$$\gamma^K(-\omega;\omega,0,0) = \gamma_{dc-Kerr}(-\omega;\omega,0,0) = \frac{3}{2}\left(\gamma^K_{//} - \gamma^K_{\perp}\right)$$

$$= \frac{1}{10}\sum_{ij}^{x,y,z}\left(3\gamma_{ijij} - \gamma_{iijj}\right) \quad \text{(S5)}$$

where $\gamma^K_{//} = \frac{1}{15}\sum_{ij}^{x,y,z}\gamma_{iijj} + 2\gamma_{ijij}$ and $\gamma^K_{\perp} = \frac{1}{15}\sum_{ij}^{x,y,z}2\gamma_{iijj} - \gamma_{ijij}$. In the Kerr experiment, absolute measurements are performed, *i.e.* absolute second hyperpolarizabilities of the sample molecules are determined without calibration with a reference molecule. [S14]

(iv) The third-harmonic scattering (THS). [S15,16] In this experiment, a scattered light is detected at the optical frequency 3ω from an intense laser pulsed at ω. The total third-order response reads:

$$\gamma_{THS}(-3\omega;\omega,\omega,\omega) = [\langle\gamma^2_{ZZZZ}\rangle + \langle\gamma^2_{ZXXX}\rangle]^{\frac{1}{2}} \quad \text{(S6)}$$

where $\langle\gamma^2_{ZZZZ}\rangle$ and $\langle\gamma^2_{ZXXX}\rangle$ are rotational averages of the γ tensor components. The relationships between these two quantities and the molecular tensor components γ_{ijkl} are determined by the scattering geometry and the polarization state of the fundamental and the harmonic light beams. In common experimental setups, the incident fundamental light beam is propagating along the Y-direction and the scattered light is collected in the X-direction of the laboratory frame. When the incident light is polarized in the Z-direction (vertical geometry) and the scattered light collected using the same polarization, the expressions of the intensity is proportional to $\langle\gamma^2_{ZZZZ}\rangle$ whereas when the incident light is polarized in the X-direction (horizontal geometry) and the scattered light remains collected using the vertical polarization, the scattering intensity is proportional to $\langle\gamma^2_{ZXXX}\rangle$. After employing Andrew and Thirunamachandran technique, these two rotational averages read: [S17]

$$\langle\gamma^2_{ZZZZ}\rangle = \frac{1}{315}\sum_{ijkl}^{x,y,z}\begin{Bmatrix} 2\gamma^2_{ijkl} + 12\gamma_{iijk}\gamma_{jllk} + 6\left(\gamma_{iijk}\gamma_{ljlk} + \gamma_{ijkl}\gamma_{jikl}\right) + \\ 3\left(\gamma_{ijjk}\gamma_{ikll} + \gamma_{iijj}\gamma_{ikll} + \gamma_{ijjk}\gamma_{kill}\right) \end{Bmatrix} \quad \text{(S7)}$$

$$\langle\gamma^2_{ZXXX}\rangle = \frac{1}{630}\sum_{ijkl}^{x,y,z}\begin{Bmatrix} 16\gamma^2_{ijkl} + 24\gamma_{ijjk}\gamma_{ikll} - 12\gamma_{iijk}\gamma_{jllk} - \\ 6\left(\gamma_{iijk}\gamma_{ljlk} + \gamma_{ijkl}\gamma_{jikl}\right) - 3\left(\gamma_{iijj}\gamma_{kllk} + \gamma_{iijj}\gamma_{ikll} + \gamma_{ijjk}\gamma_{kill}\right) \end{Bmatrix} \quad \text{(S8)}$$

They also define the depolarization ratio:

$$\mathrm{DR}_{THS} = \frac{\langle\gamma^2_{ZZZZ}\rangle}{\langle\gamma^2_{ZXXX}\rangle} \quad \text{(S9)}$$

DR_{THS} takes specific values depending on the symmetry of the molecular moiety that is responsible of the NLO responses. In the static electric field limit (Kleinman symmetry condition), the γ tensor can be decomposed into three multipolar invariants, the isotropic (J=0), the quadrupolar (J=2) and the hexadecapolar (J=4) components:[S18]

$$\left|\gamma_{J=0}\right|^2 = \frac{1}{5}\sum_{ijkl}^{x,y,z}\gamma_{iijj}\gamma_{kkll} \quad \text{(S10)}$$

$$\left|\gamma_{J=2}\right|^2 = \frac{1}{7}\sum_{ijkl}^{x,y,z}\left(6\gamma_{iijk}\gamma_{jkll} - 2\gamma_{iijj}\gamma_{kkll}\right) \quad \text{(S11)}$$

$$\left|\gamma_{J=4}\right|^2 = \frac{1}{35}\sum_{ijkl}^{x,y,z}\left(35\gamma^2_{ijkl} - 30\gamma_{iijk}\gamma_{jkll} + 3\gamma_{iijj}\gamma_{kkll}\right) \quad \text{(S12)}$$

Consequently, Eqs. (S7) and (S8) become:

$$\langle \gamma_{ZZZZ}^2 \rangle = \frac{1}{5}\left|\gamma_{J=0}\right|^2 + \frac{4}{35}\left|\gamma_{J=2}\right|^2 + \frac{8}{315}\left|\gamma_{J=4}\right|^2 \tag{S13}$$

$$\langle \gamma_{ZXXX}^2 \rangle = \frac{3}{140}\left|\gamma_{J=2}\right|^2 + \frac{1}{63}\left|\gamma_{J=4}\right|^2 \tag{S14}$$

Eqs. (S10)-(S12) allow rewriting DR_{THS} as: [S19]

$$\mathrm{DR}_{THS} = \frac{32\rho_{4/2}^2 + 235\rho_{0/2}^2 + 144}{20\rho_{4/2}^2 + 27} \tag{S15}$$

where $\rho_{0/2} = \left|\gamma_{J=0}\right| / \left|\gamma_{J=2}\right|$ and $\rho_{4/2} = \left|\gamma_{J=4}\right| / \left|\gamma_{J=2}\right|$ define the relative contributions of the spherical tensor components to the total third harmonic responses.

2. Structures and energies of *trans*/*cis* stilbenes

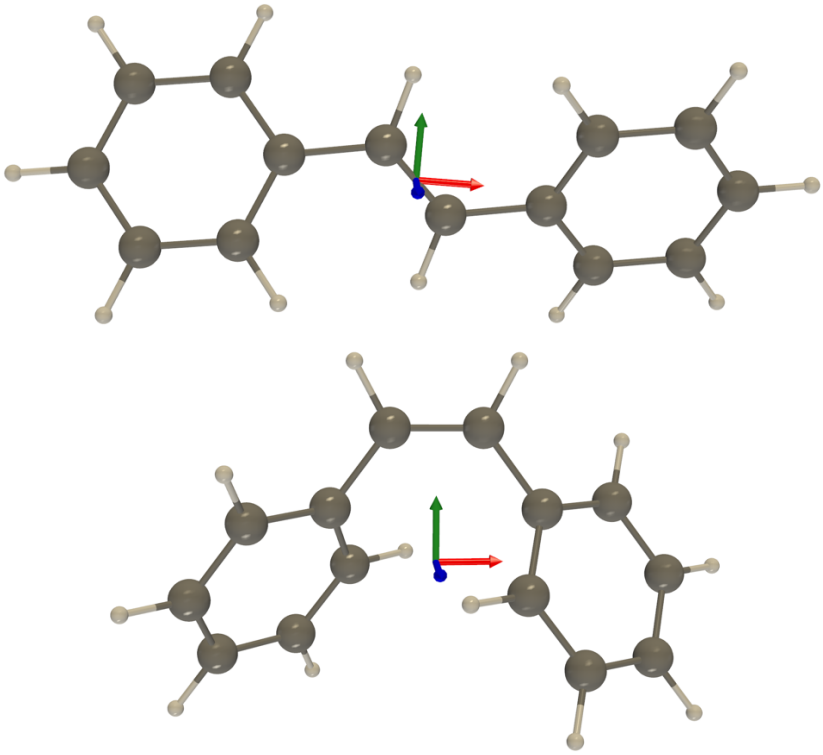

FIG S1: Optimized sturctures of the *trans*- (top) and *cis*-stilbene (bottom) isomers in the Cartesian frame: x-axis (red), y-axis (green) and z-axis (blue).

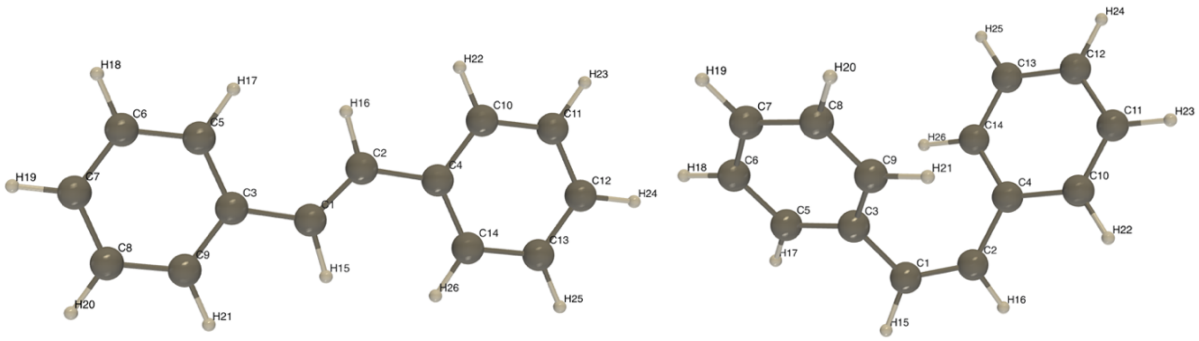

FIG S2: Atomic numbering of the *trans*- and *cis*-stilbene isomers

TABLE S1: Optimized key geometrical parameters [bond lengths (Å), bond angles (°)] and energies calculated for the *trans*- and *cis*-stilbene, as well as their differences, at the MP2/6-311G(d) level. Enthalpies and free enthalpies were evaluated at 298.15 K for P = 1 atm.

	trans	*cis*	bond length difference, Δ = d(*t*) -d(*c*)
C1—C2	1.354	1.353	0.001
C2—C4	1.468	1.476	0.008
C1—C3	1.468	1.476	0.008
C3—C5	1.409	1.406	0.003
C5—C6	1.396	1.398	0.002
C6—C7	1.400	1.399	0.001
C7—C8	1.399	1.400	0.001
C8—C9	1.397	1.396	0.001
C9—C3	1.408	1.408	0.000
C4—C10	1.408	1.406	0.002
C10—C11	1.397	1.398	0.001
C11—C12	1.399	1.399	0.000
C12—C13	1.400	1.400	0.000
C13—C14	1.396	1.396	0.000
C14—C4	1.409	1.408	0.001
C3—C5—C6	120.9	120.7	/
C1—C3—C5	119.5	119.9	/
C2—C1—C3	124.8	126.0	/
C2—C1—C3—C5 (C9)	28.4	43.4	/
C4—C2—C1—C3	179.2	5.5	/
Energy	*Trans*	*Cis*	ΔE = E(*c*) - E(*t*) (kcal/mol)
Equilibrium torsional angle (°)	28.4	43.4	/
MP2 electronic energy (a.u.)	-539.079304	-539.077920	0.87
MP2 energy + ZPVEs[a] (a.u.)	-538.867194	-538.865334	1.20
Enthalpy (H°, a.u.)	-538.854361	-538.852751	1.01
Free enthalpy (G°, a.u.)	-538.906264	-538.904056	1.38

[a] Zero point vibrational energy.

3. Numerical aspects of the calculations: integration grids and Romberg method

TABLE S2. Static second hyperpolarizabilities (a.u.) of the *trans*- and *cis*-stilbene as obtained at the DFT levels using the 4^{th}-order numerical derivative approach with either the **ultrafine** and **superfine** grids. The value in parenthesis reports the relative error (in %) with respect to superfine grid.

XCFs	**Ultrafine** (99,590)				**Superfine** (175/250,974)			
	γ_{xxxx}	$\gamma_{//}$	γ_{THS}	DR_{THS}	γ_{xxxx}	$\gamma_{//}$	γ_{THS}	DR_{THS}
				***Trans*-stilbene**				
B3LYP	612536 (0.00)	149071(0.02)	228134 (0.01)	8.7	612530	149040	228120	8.7
M06	570610 (0.01)	136506 (0.03)	211477 (0.03)	8.5	570578	136462	211414	8.5
M06-2X	435464 (0.03)	107328 (-0.02)	162573 (0.03)	8.8	435330	107348	162521	8.8
CAM-B3LYP	433340 (-0.03)	109108 (-0.05)	162702 (-0.04)	9.1	433464	109161	162765	9.1
				***Cis*-stilbene**				
B3LYP	141268 (0.001)	64840 (0.000)	73503 (0.001)	25.2	141074	64826	73453	25.2
M06	124702 (-0.003)	57007 (-0.002)	65140 (-0.002)	24.0	125108	57108	65278	24.0
M06-2X	97267 (0.003)	47163 (-0.030)	52675 (0.070)	28.6	97021	47176	52636	28.6
CAM-B3LYP	99057 (-0.001)	49902 (-0.050)	55035 (-0.060)	31.5	99123	49929	55070	31.5

TABLE S3. Romberg table of the static γ_{xxxx} (a.u.) of *trans*- (top) and *cis*-stilbene (bottom) calculated from the finite differentiation of $\mathcal{E}$. The calculations were performed at the MP2/6-311+G(d) level.

	m=0	m=1	m=2	m=3	m=4	m=5	m=6	m=7	m=8
k=0	437063	436861	437055	437192	437271	437312	437334	437344	437350
k=1	437264	436282	436092	436015	435983	435969	435963	435960	
k=2	438246	436851	**436630**	**436493**	436417	436377	436357		
k=3	439642	437513	**437593**	437630	437651	437662			
k=4	441771	437271	437335	437319	437312				
k=5	446270	437079	437446	437415					
k=6	455461	435980	437656						
k=7	474942	430952							
k=8	518932								

→ $\gamma_{xxxx} = (437 \pm 1) \times 10^3$ a.u.

	m=0	m=1	m=2	m=3	m=4	m=5	m=6	m=7	m=8
k=0	106387	104281	103101	102467	102138	101970	101885	101842	101821
k=1	108492	107823	107538	107408	107348	107320	107306	107299	
k=2	109161	108679	**108443**	**108306**	108232	108193	108173		
k=3	109643	109387	**109404**	109416	109423	109427			
k=4	109900	109333	109322	109310	109304				
k=5	110467	109367	109402	109399					
k=6	111567	109263	109421						
k=7	113872	108788							
k=8	118955								

→ $\gamma_{xxxx} = (108 \pm 1) \times 10^3$ a.u.

TABLE S4. Romberg table of the static γ_{xxxx} (a.u.) of *trans*-stilbene calculated from the finite differentiation of $\mathcal{E}$ (top), α (middle) and β (bottom). The calculations were performed at the CAM-B3LYP/6-311+G(d) level using the **superfine** integration grid.

	m=0	m=1	m=2	m=3	m=4	m=5
k=0	441105	443711	444446	444634	444681	444692
k=1	433286	432686	432636	432622	432619	
k=2	435087	433442	**433464**	**433463**		
k=3	440023	433111	**433549**			
k=4	460757	426546				
k=5	563391					

→ $\gamma_{xxxx} = (433 \pm 1) \times 10^3$ a.u.

	m=0	m=1	m=2	m=3	m=4	m=5
k=0	433511	433460	433460	433460	433460	433460
k=1	433664	433461	433462	433462	433462	
k=2	434272	433456	**433461**	**433461**		
k=3	436718	433385	**433465**			
k=4	446717	432178				
k=5	490335					

→ $\gamma_{xxxx} = (433 \pm 1) \times 10^3$ a.u.

	m=0	m=1	m=2	m=3	m=4	m=5
k=0	433562	433460	433460	433460	433460	433460
k=1	433865	433460	433460	433460	433460	
k=2	435083	433446	**433461**	**433460**		
k=3	439994	433232	**433480**			
k=4	460280	429511				
k=5	552584					

→ $\gamma_{xxxx} = (433 \pm 1) \times 10^3$ a.u.

TABLE S5. Romberg table of the static γ_{xxxx} (a.u.) of *cis*-stilbene calculated from the finite differentiation of $\mathcal{E}$ (top), α (middle) and β (bottom). The calculations were performed at the CAM-B3LYP/6-311+G(d) level using the **superfine** integration grid.

	m=0	m=1	m=2	m=3	m=4	m=5
k=0	110613	114705	115818	116102	116174	116191
k=1	98337	98007	97933	97915	97910	
k=2	99329	99109	**99111**	**99111**		
k=3	99988	99072	**99134**			
k=4	102738	98141				
k=5	116527					

$\rightarrow \gamma_{xxxx} = (99 \pm 1) \times 10^3$ a.u.

	m=0	m=1	m=2	m=3	m=4	m=5
k=0	991334	99129	99129	99129	99130	99130
k=1	99147	99120	99120	99120	99120	
k=2	99229	99120	**99121**	**99121**		
k=3	99554	99111	**99121**			
k=4	10088	98959				
k=5	106656					

$\rightarrow \gamma_{xxxx} = (99 \pm 1) \times 10^3$ a.u.

	m=0	m=1	m=2	m=3	m=4	m=5
k=0	99136	99123	99123	99123	99123	99123
k=1	99177	99122	99123	99123	99123	
k=2	99339	99121	**99123**	**99123**		
k=3	99993	99095	**99127**			
k=4	102686	98617				
k=5	114895					

$\rightarrow \gamma_{xxxx} = (99 \pm 1) \times 10^3$ a.u.

TABLE S6. Second hyperpolarizability (a.u.) of the *trans*-stilbene and *cis*-stilbene molecule calculated from the finite differentiation of $\mathcal{E}$, α and β with various DFT levels using **superfine** integration grid. The relative errors calculated with respect to the $\boldsymbol{\beta}$ differentiation are in parenthesis.

	From energy ($\mathcal{E}$)			**From alpha $\boldsymbol{\alpha(0;0)}$**			**From beta $\boldsymbol{\beta(0;0,0)}$**		
				***trans*-stilbene**					
	$\gamma_{//}$	γ_{THS}	$\mathrm{DR_{THS}}$	$\gamma_{//}$	γ_{THS}	$\mathrm{DR_{THS}}$	$\gamma_{//}$	γ_{THS}	$\mathrm{DR_{THS}}$
B3LYP	149040 (-0.01)	228120 (-0.010)	8.7	149054 (-0.003)	228124 (-0.003)	8.7	149059	228132	8.7
M06	136462 (-0.01)	211414 (-0.050)	8.5	136461 (-0.010)	211491 (-0.013)	8.5	136469	211520	8.5
M06-2X	107348 (-0.08)	162521 (-0.110)	8.8	107429 (0.001)	162687 (-0.002)	8.8	107429	162690	8.8
CAM-B3LYP	109161 (0.008)	162765 (0.005)	9.1	109151 (-0.001)	162756 (-0.001)	9.1	109152	162757	9.1
				***cis*-stilbene**					
B3LYP	64826 (-0.03)	73453 (-0.090)	25.2	64843 (-0.001)	73517 (-0.001)	25.2	64844	73518	25.2
M06	57108 (-0.16)	65278 (-0.360)	24.0	57212 (0.021)	65507 (-0.006)	24.0	57200	65511	24.0
M06-2X	47173 (-0.01)	52635 (-0.170)	28.6	47195 (0.010)	52723 (-0.002)	28.3	47190	52724	28.3
CAM-B3LYP	49929 (-0.02)	55070 (-0.010)	31.5	49936 (-0.004)	55075 (-0.001)	31.5	49938	55076	31.5

4. Basis set effects on the second hyperpolarizabilities

TABLE S7. Basis set effect on the static second hyperpolarizability (10^3 a.u.) of the *trans*-stilbene molecule. All calculations were performed with the CAM-B3LYP XCF and the superfine grid, using hybrid differentiation schemes with field-dependent polarizabilities evaluated analytically. The values in the squared brackets in the first column correspond to the number of contracted GTOs. Values in parentheses are differences (%) with respect to the reference d-aug-cc-pVTZ results.

Basis sets	γ_{xxxx}	$\gamma_{//}$	γ_{THS}	DR_{THS}
6-31G(d) [234]	347 (-21)	69 (-37)	123 (-26)	7.0 (-24)
6-311G(d) [288]	373 (-15)	77 (-31)	133 (-20)	7.4 (-20)
6-311G(d,p) [324]	375 (-15)	77 (-30)	134 (-19)	7.2 (-22)
cc-pVDZ [256]	364 (-17)	74 (-33)	130 (-22)	7.1 (-23)
cc-pVTZ [588]	382 (-13)	80 (-28)	137 (-18)	7.3 (-21)
cc-pVQZ [1130]	394 (-10)	85 (-23)	143 (-14)	7.6 (-17)
6-31+G(d) [290]	443 (1)	112 (1)	167 (0.2)	9.1 (-1)
6-311+G(d) [344]	433 (-1)	109 (-2)	163 (-2)	9.1 (-1)
6-311+G(d,p) [380]	436 (-1)	109 (-2)	163 (-2)	9.0 (-2)
aug-cc-pVDZ [430]	435 (-1)	110 (-2)	163 (-2)	9.1 (-1)
aug-cc-pVTZ [920]	437 -1)	111 (-1)	165 (-1)	9.2 (0)
aug-cc-pVQZ [1672]	439 (-0.2)	112 (0.2)	165 (-0.6)	9.2 (0)
d-aug-cc-pVDZ [604]	440 (0.1)	113 (0.9)	166 (-0.2)	9.3 (1)
d-aug-cc-pVTZ [1252]	440	112	166	9.2

TABLE S8. Basis set effect on the static second hyperpolarizability (10^3 a.u.) of the *cis*-stilbene molecule. All calculations were performed with the CAM-B3LYP XCF and the superfine grid, using hybrid differentiation schemes with field-dependent polarizabilities evaluated analytically. The values in the squared brackets in the first column correspond to the number of contracted GTOs. Values in parentheses are differences (%) with respect to the reference d-aug-cc-pVTZ results.

Basis sets	γ_{xxxx}	$\gamma_{//}$	γ_{THS}	DR_{THS}
6-31G(d) [234]	59 (-43)	20 (-61)	27 (-52)	11.5 (-63)
6-311G(d) [288]	66 (-36)	24 (-52)	32 (-44)	13.7 (-56)
6-311G(d,p) [324]	66 (-36)	24 (-52)	32 (-44)	13.6 (-56)
cc-pVDZ [256]	64 (-39)	23 (-56)	30 (-47)	12.9 (-58)
cc-pVTZ [588]	69 (-33)	26 (-49)	33 (-42)	14.6 (-53)
cc-pVQZ [1130]	75 (-28)	31 (-41)	37 (-34)	17.3 (-44)
6-31+G(d) [290]	102 (-1)	52 (2)	57 (1)	32.8 (6)
6-311+G(d) [344]	99 (-5)	50 (-3)	55 (-3)	31.5 (2)
6-311+G(d,p) [380]	99 (-4)	50 (-3)	55 (-3)	31.3 (1)
aug-cc-pVDZ [430]	102 (-2)	51 (-1)	56 (-2)	31.4 (1)
aug-cc-pVTZ [920]	103 (-1)	51 (0.1)	57 (-0.4)	31.2 (0.6)
aug-cc-pVQZ [1672]	103 (-1)	52 (1)	57 (0.4)	32.8 (6)
d-aug-cc-pVDZ [604]	104 (1)	53 (3)	58 (2)	33.3 (7)
d-aug-cc-pVTZ [1252]	104	51	57	31.0

TABLE S9. Basis set effect on the γ(trans)/γ(cis) ratio of stilbene molecules. All calculations were performed with the CAM-B3LYP XCF and the superfine grid, using hybrid differentiation schemes with field-dependent polarizabilities evaluated analytically. The values in the squared brackets in the first column correspond to the number of contracted GTOs.

Basis sets	γ_{xxxx}	$\gamma_{//}$	γ_{THS}	DR_{THS}
6-31G(d) [234]	5.85	3.50	4.52	0.61
6-311G(d) [288]	5.60	3.16	4.22	0.54
6-311G(d,p) [324]	5.64	3.17	4.24	0.53
cc-pVDZ [256]	5.71	3.28	4.33	0.55
cc-pVTZ [588]	5.52	3.07	4.13	0.50
cc-pVQZ [1130]	5.24	2.81	3.84	0.44
6-31+G(d) [290]	4.33	2.15	2.90	0.28
6-311+G(d) [344]	4.37	2.19	2.96	0.29
6-311+G(d,p) [380]	4.39	2.19	2.96	0.29
aug-cc-pVDZ [430]	4.26	2.16	2.92	0.29
aug-cc-pVTZ [920]	4.25	2.16	2.90	0.29
aug-cc-pVQZ [1672]	4.26	2.15	2.90	0.28
d-aug-cc-pVDZ [604]	4.21	2.13	2.87	0.28
d-aug-cc-pVTZ [1252]	4.24	2.17	2.93	0.29

5. Electron correlation effects on the second hyperpolarizabilities

TABLE S10. The γ(trans)/γ(cis) ratio of stilbene molecules as obtained with wavefunction methods using the 4^{th}-order numerical derivative approach and the 6-311+G(d) basis set. The values in the parentheses show the relative error with respect to the CCSD(T) reference values.

Methods	$\gamma_{//}$	γ_{THS}	DR_{THS}
HF	1.96 (-2)	2.59 (-2)	0.21 (-22)
MP2	2.08 (4)	2.76 (4)	0.28 (4)
MP3	2.03 (1)	2.67 (1)	0.28 (4)
MP4D	2.05 (2)	2.66 (0)	0.30 (11)
MP4DQ	2.00 (0)	2.61 (-2)	0.28 (4)
MP4SDQ	2.04 (2)	2.70 (2)	0.27 (0)
MP4	2.11 (5)	2.80 (6)	0.28 (4)
CCSD	1.98 (-1)	2.61 (-2)	0.26 (-4)
CCSD(T)	**2.00**	**2.65**	**0.27**

6. Selecting an XCF for computing the second hyperpolarizabilities

6.1. Conventional XCFs

TABLE S11. γ(trans)/γ(cis) ratios of the static second hyperpolarizability of the stilbene molecule, as obtained using various DFT XCFs and the 2nd order numerical derivative approach. All calculations were performed using the 6-311+G(d) basis set and the superfine grid. The values in parentheses show the relative error with respect to the CCSD(T)/6-311+G(d) reference values (last line), obtained using the 4^{th} order numerical derivative approach.

XCFs	$\boldsymbol{\gamma_{//}}$	$\boldsymbol{\gamma_{THS}}$	DR_{THS}
SVWN	2.37 (19)	3.15 (19)	0.41 (52)
BLYP	2.31 (16)	3.09 (17)	0.38 (41)
PBE	2.33 (17)	3.12 (18)	0.39 (44)
B97-D	2.33 (17)	3.12 (18)	0.39 (44)
M06-L	2.62 (31)	3.51 (32)	0.43 (59)
B3LYP	2.30 (15)	3.10 (17)	0.35 (30)
PBE0	2.31 (16)	3.13 (18)	0.34 (26)
M06	2.39 (20)	3.23 (22)	0.36 (33)
M06-2X	2.28 (14)	3.09 (17)	0.31 (15)
M06-HF	2.03 (1)	2.72 (3)	0.25 (-7)
M11	2.24 (12)	3.05 (15)	0.30 (11)
MN15	2.24 (12)	3.02 (14)	0.31 (15)
ωB97	2.12 (6)	2.85 (8)	0.26 (-4)
ωB97X	2.08 (4)	2.78 (5)	0.26 (-4)
ωB97X-D	2.11 (5)	2.82 (6)	0.29 (7)
LC-ωPBE	2.18 (9)	2.95 (11)	0.27 (0)
CAM-B3LYP	2.19 (10)	2.95 (11)	0.29 (7)
LC-BLYP	2.12 (6)	2.87 (8)	0.25 (-7)
PBE0DH	2.49 (25)	3.45 (30)	0.25 (-7)
mPW2PLYP	2.24 (12)	3.03 (14)	0.31 (15)
B2-PLYP	2.24 (12)	3.03 (14)	0.31 (15)
CCSD(T)	**2.00**	**2.65**	**0.27**

TABLE S12. Isotropic (J = 0) , quadrupolar (J = 2), and hexadecapolar (J = 4) components to the second hyperpolarizability calculated at different levels of approximation using the superfine integration grid.

Methods	(J = 0) (a.u.)	(J = 2) (a.u.)	(J = 4) (a.u.)
	trans-stilbene		
SVWN	407750	564620	342270
B3LYP	333302	444805	268449
M06-2X	240215	314572	190429
CAM-B3LYP	241346	306332	185226
LC-BLYP	181940	224305	136972
HF	166961	191249	117870
MP2	258697	312586	177672
CCSD(T)	241259	287852	163316
	cis-stilbene		
SVWN	172474	124236	55492
B3LYP	144992	91130	42088
M06-2X	105531	61810	28635
CAM-B3LYP	111660	60935	29408
LC-BLYP	85814	42294	21539
HF	85355	34644	21254
MP2	123706	64259	29660
CCSD(T)	120151	60864	26467

6.2. Optimal tuning of the range-separating parameter

The range-separating parameters μ were optimized by imposing that the Koopmans theorem for the first ionization energy is satisfied. In that case, the following function, $\Delta_{\mathrm{IP}}(\mu)$ must be as close as possible to zero:

$$\Delta_{\mathrm{IP}}(\mu) = \varepsilon_{\mathrm{HOMO}}^{\mathrm{N}}(\mu) - [(\mathcal{E}(\mu, \mathrm{N}) - \mathcal{E}(\mu, \mathrm{N}-1)] \quad \text{(S16)}$$

with $\varepsilon_{\mathrm{HOMO}}^{\mathrm{N}}$, the energy of the HOMO of the N-electron system and $\mathcal{E}(\mathrm{N})$ and $\mathcal{E}(\mathrm{N}-1)$ the total ground state energies of the systems with N and N-1 electrons. In this work, μ was varied in the gas phase for the LC-BLYP, CAM-B3LYP and ωB97 XCFs to monitor the $\Delta_{\mathrm{IP}}(\mu)$ function (Table S13). Since it is known that functionals that are tuned in this manner also tend to lead to a smaller Kohn-Sham delocalization error (DE) or self-interaction error (with more reliable predictions of properties that are sensitive to the DE), the performance of DFT functionals were also rationalized by analyzing their DE. Note that the DE manifests in a curvature of $\mathcal{E}(\mathrm{N})$ versus N between integer N[S20] as defined through the following expression: [S21]

$$\begin{aligned}\Delta\mathcal{E}(\delta) &= \Delta\mathcal{E}\delta + \left\{\left[\left(\varepsilon_{\mathrm{LUMO}}^{\mathrm{N}} - \Delta\mathcal{E}\right)(1-\delta) + (\Delta\mathcal{E} - \varepsilon_{\mathrm{HOMO}}^{\mathrm{N+1}})\delta\right]\delta(1-\delta)\right\} \\ &= \Delta\mathcal{E}\delta + \Delta\Delta\mathcal{E}(\delta)\end{aligned} \quad \text{(S17)}$$

where $\delta \in [0, 1]$ defines the number of electrons that is added or removed from the system and $\Delta\mathcal{E} = \mathcal{E}(\mathrm{N}+1) - \mathcal{E}(\mathrm{N})$. $\varepsilon_{\mathrm{LUMO}}^{\mathrm{N}}$ ($\varepsilon_{\mathrm{HOMO}}^{\mathrm{N+1}}$) is the energy of the LUMO (HOMO) of the N (N+1)-electron system and $\Delta\Delta\mathcal{E}(\delta)$ related to the expression in the curly brackets, defines the deviation with respect to the linear behavior in δ, as described by $\Delta\mathcal{E}\delta$. Eq. (S17) has already been employed to quantify the localization and delocalization errors at the HF and DFT levels. [S20,22–24] While the μ-tuning scheme of eq. S16 has been demonstrated to offer the possibility to describe accurately the molecular responses to electric fields, [S25,26] some controversial conclusions were also reported [S27,28] leading to a new tuning procedure definition proposed by Besalú-Sala *et al.* [S29], T_{α} −LC-BLYP dedicated specifically to the calculation of second hyperpolarizabilities. The details of the procedure can be found in Ref. [S29]

TABLE S13. Ionization energy calculated for *trans*-stilbene and *cis*-stilbene molecules by tuning the range-separated parameter μ in view of satisfying Koopmans' theorem.

μ (bohr^{-1})	ε^{N}_{HOMO} (eV)	$\mathcal{E}(\mu, N)$ (a.u.)	$\mathcal{E}(\mu, N-1)$ (a.u.)	$\Delta_{IP}(\mu)$ (eV)
		***trans*-stilbene**		
		LC-BLYP		
0.48	-8.589	-539.1096551	-538.8167815	-0.620
0.47	-8.573	-539.1206672	-538.8278971	-0.606
0.40	-8.424	-539.2011886	-538.9098811	-0.497
0.33	-8.193	-539.2904914	-539.0022598	-0.350
0.26	-7.846	-539.3975261	-539.1144043	-0.142
0.19	-7.338	-539.5422019	-539.2665425	0.163
0.12	-6.652	-539.7645902	-539.4971650	0.625
0.10	-6.419	-539.8518517	-539.5866113	0.798
0.05	-5.754	-540.1331380	-539.8704300	1.395
		ωB97		
0.48	-8.541	-540.6346695	-540.3447030	-0.651
0.40	-8.359	-540.6990360	-540.4112344	-0.528
0.33	-8.108	-540.7570917	-540.4730569	-0.379
0.30	-7.965	-540.7841221	-540.5023903	-0.299
0.28	-7.856	-540.8035719	-540.5236374	-0.239
0.19	-7.186	-540.9205530	-540.6515587	0.134
0.12	-6.417	-541.0841752	-540.8264683	0.595
0.10	-6.153	-541.1527521	-540.8983407	0.770
0.05	-5.420	-541.3912695	-541.1435947	1.319
		CAM-B3LYP		
0.48	-7.363	-540.4159933	-540.1331998	0.332
0.40	-7.291	-540.4579546	-540.1759664	0.382
0.33	-7.188	-540.4988590	-540.2183291	0.445
0.26	-7.031	-540.5479484	-540.2698202	0.537
0.19	-6.787	-540.6143830	-540.3401798	0.674
0.12	-6.477	-540.7167578	-540.4460470	0.889
0.10	-6.368	-540.7569300	-540.4872097	0.971
0.05	-6.056	-540.8902370	-540.6224590	1.231

		***cis*-stilbene**		
		LC-BLYP		
0.48	-8.826	-539.1050985	-538.8017925	-0.573
0.47	-8.809	-539.1161162	-538.8130085	-0.561
0.40	-8.650	-539.1966645	-538.8957214	-0.461
0.33	-8.409	-539.2859614	-538.9888446	-0.324
0.26	-8.051	-539.3929212	-539.1016471	-0.125
0.19	-7.534	-539.5373450	-539.2540084	0.176
0.12	-6.813	-539.7590784	-539.4849147	0.647
0.10	-6.566	-539.8460407	-539.5743355	0.827
0.05	-5.873	-540.1347072	-539.8675105	1.398
		ωB97		
0.48	-8.761	-540.6310765	-540.3311398	-0.599
0.40	-8.569	-540.6953944	-540.3983756	-0.487
0.33	-8.309	-540.7533397	-540.4608224	-0.349
0.30	-8.161	-540.7802895	-540.4904003	-0.273
0.26	-7.923	-540.8206749	-540.5350242	-0.150
0.19	-7.367	-540.9160729	-540.6399213	0.147
0.12	-6.584	-541.0787228	-540.8139725	0.620
0.05	-5.588	-541.3844798	-541.1288047	1.369
		CAM-B3LYP		
0.48	-7.607	-540.4101832	-540.1169602	0.372
0.40	-7.528	-540.4521503	-540.1600982	0.419
0.33	-7.419	-540.4930316	-540.2028040	0.478
0.30	-7.356	-540.5126578	-540.2234928	0.512
0.26	-7.255	-540.5420498	-540.2545914	0.567
0.19	-7.016	-540.6083692	-540.3246811	0.703
0.12	-6.679	-540.7103776	-540.4310186	0.923
0.05	-6.243	-540.8833412	-540.6071157	1.273

TABLE S14. Static second hyperpolarizability (10^3 a.u.) as a function of the range-separating parameter (μ) for the *trans*-stilbene molecule.

μ (bohr^{-1})	$\gamma_{//}$	γ_{THS}	DR_{THS}
	ωB97		
0.05	169.2 (57)	264.0 (70)	8.4 (-15)
0.12	144.4 (34)	217.9 (40)	8.8 (-11)
0.19	120.7 (12)	178.1 (14)	9.3 (-6)
0.22	112.7 (4)	165.4 (7)	9.3 (-6)
0.28	100.1 (-7)	146.2 (-6)	9.4 (-5)
0.30	96.8 (-10)	141.3 (-9)	9.4 (-5)
0.33	92.5 (-14)	135.0 (-13)	9.4 (-5)
0.40	84.8 (-21)	123.7 (-20)	9.4 (-5)
0.48	78.9 (-27)	115.2 (-26)	9.4 (-5)
	CAM-B3LYP		
0.05	149.5 (38)	228.0 (47)	8.7 (-12)
0.12	138.0 (28)	208.2 (34)	8.9 (-10)
0.19	125.2 (16)	187.4 (21)	9.0 (-9)
0.28	113.5 (5)	169.4 (9)	9.1 (-8)
0.33	109.1 (1)	162.7 (5)	9.1 (-8)
0.40	104.6 (-3)	155.9 (0.6)	9.1 (-8)
0.48	100.9 (-6)	150.5 (-3)	9.1 (-8)
	LC-BLYP		
0.47	81.4 (-25)	119.3 (-23)	9.3 (-6)
0.40	86.9 (-19)	127.3 (-18)	9.3 (-6)
0.33	96.0 (-12)	139.4 (-10)	9.4 (-5)
0.30	99.7 (-8)	146.3 (-6)	9.3 (-6)
0.26	107.5 (-0.5)	157.8 (2)	9.3 (-6)
0.23	115.0 (6)	169.0 (9)	9.3 (-6)
0.19	126.5 (17)	187.0 (21)	9.2 (-7)
0.12	154.9 (43)	232.5 (50)	9.0 (-9)
0.10	164.6 (52)	248.6 (60)	8.9 (-10)
0.05	185.8 (72)	285.6 (84)	8.6 (-13)
CCSD(T)	**108.0**	**155.0**	**9.9**

TABLE S15. Static second hyperpolarizability (10^3 a.u.) as a function of the range-separating parameter (μ) for the *cis*-stilbene molecule.

XCFs	$\gamma_{//}$	γ_{THS}	DR_{THS}
	ωB97		
0.05	70.4 (30)	82.3 (41)	21.0 (-43)
0.12	65.7 (22)	74.3 (27)	25.9 (-30)
0.19	57.0 (6)	63.0 (8)	31.3 (-15)
0.22	56.4 (4)	61.9 (6)	33.0 (-10)
0.26	49.4 (-8)	54.0 (-8)	35.5 (-3)
0.30	46.0 (-15)	50.2 (-14)	35.5 (-3)
0.33	43.9 (-19)	47.7 (-18)	36.0 (-2)
0.40	40.0 (-26)	43.4 (-26)	36.7 (-0.3)
0.48	37.0 (-31)	40.2 (-31)	37.2 (1)
	CAM-B3LYP		
0.05	65.9 (22)	74.5 (27)	25.6 (-30)
0.12	62.7 (16)	70.3 (20)	27.6 (-25)
0.19	57.6 (7)	64.0 (9)	29.6 (-19)
0.26	53.2 (-1)	58.8 (0.5)	30.8 (-16)
0.30	51.2 (-5)	56.5 (-3)	31.3 (-15)
0.33	49.9 (-8)	55.1 (-6)	31.5 (-14)
0.40	47.7 (-11)	52.5 (-10)	31.9 (-13)
0.48	45.9 (-15)	50.5 (-14)	32.2 (-12)
	LC-BLYP		
0.47	38.4 (-29)	41.6 (-29)	36.9 (0.3)
0.40	41.1 (-24)	44.7 (-24)	36.4 (-1)
0.33	45.2 (-16)	49.3 (-16)	35.6 (-3)
0.30	47.6 (-12)	51.9 (-11)	35.1 (-5)
0.26	51.5 (-5)	56.3 (-4)	34.2 (-7)
0.23	55.0 (2)	60.4 (3)	33.3 (-9)
0.19	60.8 (13)	67.1 (15)	31.5 (-14)
0.12	73.4 (36)	82.4 (41)	27.1 (-26)
0.10	77.0 (43)	87.1 (49)	25.7 (-30)
0.05	82.8 (53)	95.3 (63)	22.9 (-38)
CCSD(T)	**54.0**	**58.5**	**36.8**

6.3. Tuning the HF exchange and the PT2 correlation in B2-BLYP

TABLE S16. B2-PLYP/6-311+G(d) static second hyperpolarizabilities (10^3 a.u.) of *trans*-stilbene as a function of the percentage of PT2 correlation (for a percentage of HF exchange fixed at 53%) and as a function of the percentage of HF exchange (for a percentage of PT2 correlation fixed at 27%). The values in parentheses are the relative errors in % with respect to the reference CCSD(T) values.

% **PT2**	$\gamma_{//}$	γ_{THS}	DR_{THS}
0	105.0 (-3)	156.0 (1)	9.1 (-8)
5	110.6 (2)	165.1 (7)	9.0 (-9)
10	116.1 (7)	173.8 (12)	9.0 (-9)
15	121.7 (13)	182.4 (18)	9.0 (-9)
20	127.2 (18)	191.1 (23)	9.0 (-9)
25	132.9 (23)	200.0 (29)	9.0 (-9)
35	144.2 (34)	217.5 (40)	8.9 (-10)
45	155.8 (44)	235.3 (52)	8.9 (-10)
55	167.4 (55)	253.3 (63)	8.9 (-10)
65	179.3 (66)	271.5 (75)	8.9 (-10)
75	191.3 (77)	290.0 (87)	8.9 (-10)
85	203.5 (88)	308.5 (99)	8.9 (-10)
90	209.7 (94)	317.8 (105)	8.9 (-10)
100	222.2 (106)	336.7 (117)	8.9 (-10)
% **HF**	$\gamma_{//}$	γ_{THS}	DR_{THS}
0	324.3 (200)	512.3 (231)	8.3 (-16)
10	264.1 (145)	413.3 (167)	8.4 (-15)
15	240.7 (123)	374.8 (142)	8.5 (-14)
20	220.4 (104)	341.7 (120)	8.5 (-14)
27	196.3 (82)	302.4 (95)	8.6 (-13)
37	168.4 (56)	257.1 (66)	8.7 (-12)
47	146.3 (35)	221.4 (43)	8.9 (-10)
55	131.7 (22)	198.0 (28)	9.0 (-9)
60	123.7 (15)	185.1 (19)	9.0 (-9)
70	110.0 (2)	163.1 (5)	9.2 (-7)
80	98.5 (-9)	144.9 (-7)	9.3 (-6-
100	80.7 (-25)	117.0 (-25)	9.6 (-3)

TABLE S17. B2-PLYP/6-311+G(d) static second hyperpolarizabilities (10^3 a.u.) of *cis*-stilbene as a function of the percentage of PT2 correlation (for a percentage of HF exchange fixed at 53%) and as a function of the percentage of HF exchange (for a percentage of PT2 correlation fixed at 27%). The values in parentheses are the relative errors in % with respect to the reference CCSD(T) values.

% **PT2**	$\gamma_{//}$	γ_{THS}	DR_{THS}
0	48.0 (-11)	52.8 (-10)	32.1 (-13)
10	52.4 (-3)	58.0 (-1)	30.6 (-17)
15	54.7 (1)	60.6 (4)	30.1 (-18)
20	57.0 (6)	63.3 (8)	29.5 (-20)
25	59.3 (10)	66.0 (13)	29.1 (-21)
35	64.0 (19)	71.5 (22)	28.3 (-23)
45	68.8 (27)	77.1 (32)	27.5 (-26)
55	73.8 (37)	82.8 (42)	27.3 (-27)
65	78.9 (46)	88.7 (52)	26.9 (-27)
75	84.1 (56)	94.7 (62)	26.7 (-28)
85	89.5 (66)	100.9 (72)	26.5 (-28)
90	92.2 (71)	104.0 (78)	26.4 (-29)
100	97.8 (81)	110.4 (89)	26.3
% **HF**	$\gamma_{//}$	γ_{THS}	DR_{THS}
0	132.8 (146)	158.5 (171)	18.7 (-49)
10	109.6 (103)	128.5 (120)	20.5 (-44)
15	100.6 (86)	117.0 (100)	21.4 (-42)
20	92.8 (72)	107.2 (83)	22.4 (-39)
27	83.6 (55)	95.7 (64)	23.7 (-36)
37	72.9 (35)	82.5 (41)	25.7 (-30)
47	64.5 (19)	72.2 (23)	27.7 (-25)
53	60.2 (11)	67.1 (15)	28.9 (-21)
60	55.8 (3)	61.8 (6)	30.4 (-17)
70	50.5 (-6)	55.5 (-5)	32.5 (-12)
80	46.0 (-15)	50.2 (-14)	34.6 (-6)
90	42.1 (-22)	45.8 (-22)	36.8 (0)
100	31.8 (-41)	42.0 (-28)	39.0 (6)

6.4. Delocalization errors with exchange correlation functionals

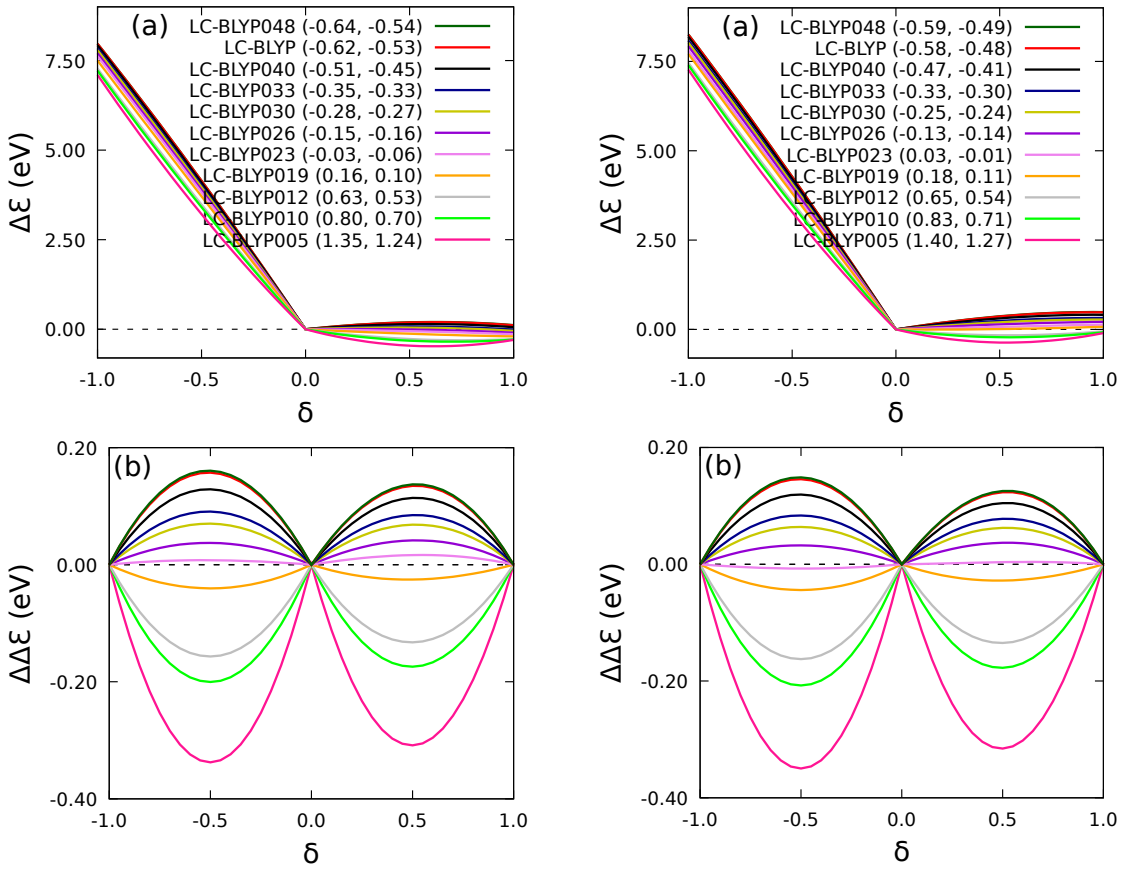

FIG. S3. For different values of μ in the LC-BLYP XC functional, (a) electronic energy of *trans*-stilbene (left) and *cis*-stilbene (right) as a function of the fractional electron number (δ) where $\delta = 0$ corresponds to the neutral system having $\Delta E = 0$; and (b) $\Delta\Delta E(\delta)$ deviation from the linear interpolation as a function of δ for *trans*-stilbene (left) and *cis*-stilbene (right). The quantities in parentheses are the coefficients of the δ^2 term (eV), describing the curvature of the deviation, for the $-1 \leq \delta \leq 0$ and $0 \leq \delta \leq 1$ intervals. All calculations were carried out using the 6-311+G(d) basis set.

TABLE S18. Relative error on the second hyperpolarizabilities of *trans*-stilbene as a function of the average curvature coefficient (eV) as obtained at different levels of approximation. All DFT calculations were performed with the superfine integration grid.

Methods	Coefficients	Relative error on $\gamma_{//}$	Relative error on γ_{THS}	Relative error on DR_{THS}
HF	-1.00	-31	-32	2
SVWN	2.17	69	84	-15
BLYP	1.98	77	91	-14
PBE	2.02	71	85	-14
B97-D	2.00	71	85	-14
M06-L	1.97	42	58	-19
B3LYP	1.50	38	47	-12
PBE0	1.36	27	35	-12
M06	1.36	26	36	-14
M06-2X	0.70	-1	5	-11
M06-HF	-0.42	-24	-23	-3
M11	-0.31	-19	-15	-10
MN15	0.94	11	16	-9
ωB97	-0.51	-21	-20	-5
ωB97X	-0.38	-15	-13	-4
ωB97X-D	-0.11	-4	-2	-6
LC-ωPBE	-0.53	-24	-22	-7
CAM-B3LYP	0.44	1	5	-8
LC-BLYP	-0.58	-25	-23	-6
LC-BLYP040	-0.48	-19	-18	-6
LC-BLYP033	-0.34	-12	-10	-5
LC-BLYP030	-0.28	-8	-6	-6
LC-BLYP026	-0.16	-0.5	2	-6
LC-BLYP023	-0.05	6	9	-6
LC-BLYP019	0.13	17	21	-7
LC-BLYP012	0.58	43	50	-9
LC-BLYP010	0.75	52	60	-10
LC-BLYP005	1.30	72	84	-13

TABLE S19. Relative error on the second hyperpolarizabilities of *cis*-stilbene as a function of the average curvature coefficient (eV) as obtained at different levels of approximation. All DFT calculations were performed with the superfine integration grid.

Methods	Coefficients	Relative error on $\gamma_{//}$	Relative error on γ_{THS}	Relative error on DR_{THS}
HF	-0.80	-29	-31	33
SVWN	2.12	43	55	-44
BLYP	1.98	54	64	-40
PBE	2.02	47	58	-41
B97-D	2.55	47	57	-41
M06-L	2.03	8	19	-49
B3LYP	1.54	20	26	-32
PBE0	1.39	9	14	-31
M06	1.36	6	12	-36
M06-2X	0.73	-13	-10	-23
M06-HF	-0.29	-25	-25	4
M11	-0.17	-28	-26	-18
MN15	0.97	-1	2	-21
ωB97	-0.47	-26	-26	0
ωB97X	-0.35	-18	-18	0
ωB97X-D	-0.09	-9	-8	-11
LC-ωPBE	-0.49	-30	-30	-6
CAM-B3LYP	0.47	-8	-6	-14
LC-BLYP	-0.53	-29	-29	0.3
LC-BLYP040	-0.44	-24	-14	-1
LC-BLYP033	-0.32	-16	-16	-3
LC-BLYP030	-0.25	-12	-11	-5
LC-BLYP026	-0.14	-5	-4	-7
LC-BLYP023	0.10	2	3	-9
LC-BLYP019	0.15	13	15	-14
LC-BLYP012	0.60	36	41	-26
LC-BLYP010	0.77	43	49	-30
LC-BLYP005	1.34	53	63	-38

7. Solvent effects and frequency dispersion

7.1. Geometries and thermodynamic data

TABLE S20. Torsional angle (C2–C1–C3–C5, see Figure S2) and energies of *trans*- and *cis*-stilbene as calculated at the SMD//MP2/6-311G(d) level in different solvents. Enthalpy and free enthalpy were evaluated at 298.15 K. The values in parenthesis are the relative energies between the liquid and gas phases.

1,2-DCE			
	trans-stilbene	*cis*-stilbene	ΔE = E(*c*) - E(*t*) (kcal/mol)
Equilibrium torsional angle (°)	24.6	43.6	/
Electronic energy (a.u.)	-539.099740	-539.096646	1.94 (1.07)
Enthalpy (H°, a.u.)	-538.874999	-538.871686	2.08 (1.07)
Free enthalpy (G°, a.u.)	-538.926706	-538.923253	2.17 (0.79)
THF			
Equilibrium torsional angle (°)	25.0	43.6	/
Electronic energy (a.u.)	-539.0970961	-539.094237	1.79 (0.92)
Enthalpy (H°, a.u.)	-538.872290	-538.869239	1.91 (0.90)
Free enthalpy (G°, a.u.)	-538.923950	-538.920797	1.98 (0.60)
Chloroform			
Equilibrium torsional angle (°)	25.5	43.5	/
Electronic energy (a.u.)	-539.099419	-539.096583	1.78 (0.91)
Enthalpy (H°, a.u.)	-538.874572	-538.871556	1.89 (0.88)
Free enthalpy (G°, a.u.)	-538.926216	-538.923099	1.96 (0.58)
Benzene			
Equilibrium torsional angle (°)	25.5	43.3	/
Electronic energy (a.u.)	-539.096795	-539.094304	1.56 (0.69)
Enthalpy (H°, a.u.)	-538.871824	-538.869155	1.67 (0.66)
Free enthalpy (G°, a.u.)	-538.923564	-538.920639	1.84 (0.46)

TABLE S21. Optimized key geometrical parameters [bond lengths (Å), bond angles (°)] for *trans*- and *cis*-stilbene calculated at the SMD(1,2-DCE)//MP2/6-311G(d) level. The values in parenthesis are the differences between the geometrical parameter in 1,2-dichloroethane and the ones in gas phase.

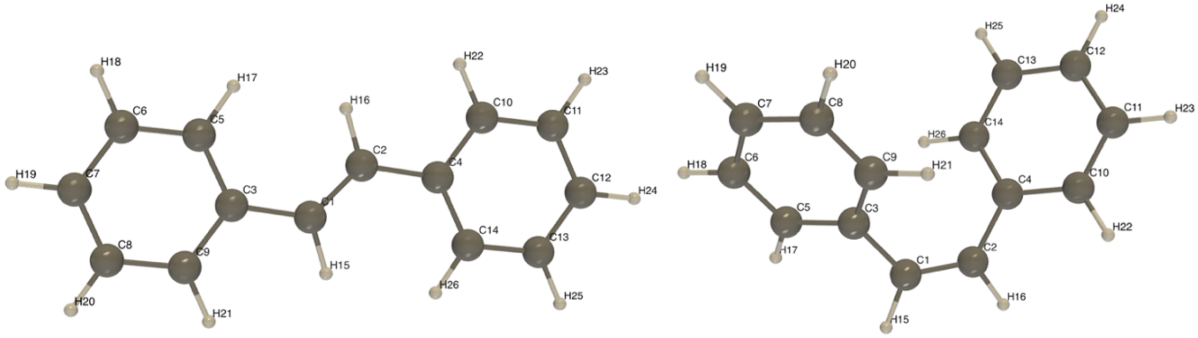

	trans	*cis*	bond length difference, Δ = d(*t*) -d(*c*)
C1—C2	1.355 (0.001)	1.354 (0.001)	0.001
C2—C4	1.469 (0.001)	1.477 (0.001)	-0.008
C1—C3	1.469 (0.001)	1.477 (0.001)	-0.008
C3—C5	1.410 (0.001)	1.407 (0.001)	0.003
C5—C6	1.397 (0.001)	1.399 (0.001)	-0.002
C6—C7	1.401 (0.001)	1.400 (0.001)	0.001
C7—C8	1.400 (0.001)	1.401 (0.001)	-0.001
C8—C9	1.398 (0.001)	1.398 (0.002)	0.000
C9—C3	1.409 (0.001)	1.409 (0.001)	0.000
C4—C10	1.409 (0.001)	1.407 (0.001)	0.002
C10—C11	1.398 (0.001)	1.399 (0.001)	-0.001
C11—C12	1.400 (0.001)	1.400 (0.001)	0.000
C12—C13	1.401 (0.001)	1.401 (0.001)	0.000
C13—C14	1.397 (0.001)	1.398 (0.002)	-0.001
C14—C4	1.410 (0.001)	1.409 (0.001)	0.001
C3—C5—C6	120.6 (-0.300)	120.7 (0.00)	/
C1—C3—C5	122.5 (3.00)	119.8 (-0.1)	/
C2—C1—C3	124.8 (0.00)	126.2 (0.20)	/
C2—C1—C3—C5	24.6 (-3.80)	43.6 (0.2)	/
C4—C2—C1—C3	179.4 (0.20)	5.4 (-0.1)	/

TABLE S22. Optimized key geometrical parameters [bond lengths (Å), bond angles (°)] for *trans*- and *cis*-stilbene calculated at the SMD(THF)//MP2/6-311G(d) level. The values in parenthesis are the differences between the geometrical parameter in THF and the ones in gas phase.

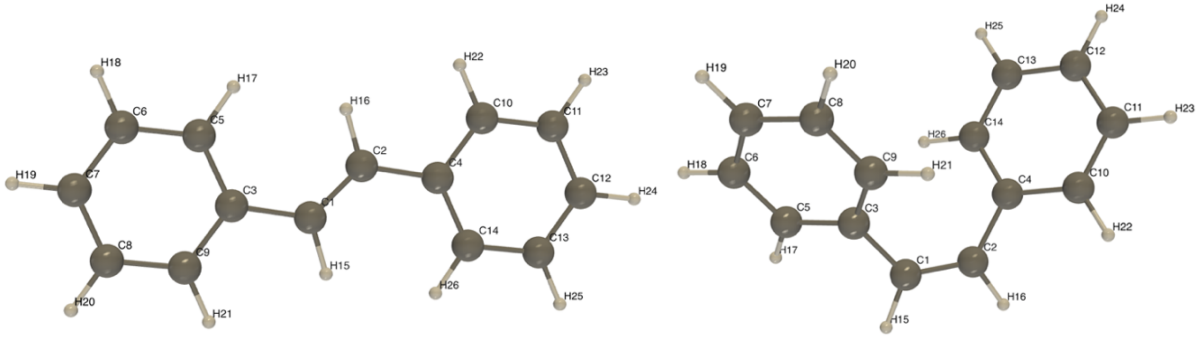

	trans	*cis*	bond length difference, Δ = d(*t*) -d(*c*)
C1—C2	1.355 (0.001)	1.354 (0.001)	0.001
C2—C4	1.469 (0.001)	1.476 (0.000)	-0.007
C1—C3	1.469 (0.001)	1.476 (0.000)	-0.007
C3—C5	1.410 (0.001)	1.407 (0.001)	0.003
C5—C6	1.397 (0.001)	1.399 (0.001)	-0.002
C6—C7	1.401 (0.001)	1.400 (0.001)	0.001
C7—C8	1.400 (0.001)	1.401 (0.001)	-0.001
C8—C9	1.398 (0.001)	1.398 (0.002)	0.000
C9—C3	1.409 (0.001)	1.408 (0.000)	0.001
C4—C10	1.409 (0.001)	1.407 (0.001)	0.002
C10—C11	1.398 (0.001)	1.399 (0.001)	-0.001
C11—C12	1.400 (0.001)	1.400 (0.001)	0.000
C12—C13	1.401 (0.001)	1.401 (0.001)	0.000
C13—C14	1.397 (0.001)	1.398 (0.002)	-0.001
C14—C4	1.410 (0.001)	1.408 (0.000)	0.002
C3—C5—C6	120.6 (-0.300)	120.7 (0.00)	/
C1—C3—C5	122.4 (2.90)	119.8 (-0.1)	/
C2—C1—C3	124.8 (0.00)	126.2 (0.20)	/
C2—C1—C3—C5	25.0 (-3.40)	43.6 (0.2)	/
C4—C2—C1—C3	179.3 (0.10)	5.4 (-0.1)	/

TABLE S23. Optimized key geometrical parameters [bond lengths (Å), bond angles (°)] for *trans*- and *cis*-stilbene calculated at the SMD(chloroform)//MP2/6-311G(d) level. The values in parenthesis are the differences between the geometrical parameter in chloroform and the ones in gas phase.

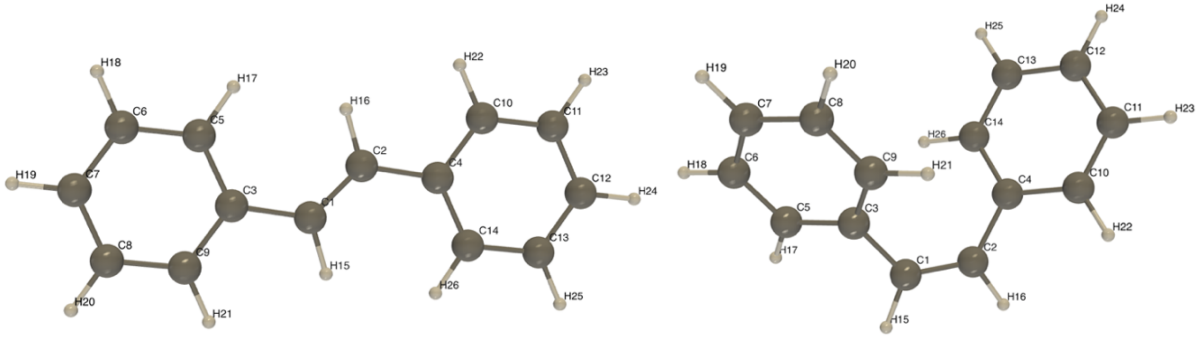

	trans	*cis*	bond length difference, Δ = d(*t*) -d(*c*)
C1—C2	1.355 (0.001)	1.354 (0.001)	0.001
C2—C4	1.469 (0.001)	1.476 (0.000)	-0.007
C1—C3	1.469 (0.001)	1.476 (0.000)	-0.007
C3—C5	1.410 (0.001)	1.407 (0.001)	0.003
C5—C6	1.397 (0.001)	1.399 (0.001)	-0.002
C6—C7	1.401 (0.001)	1.400 (0.001)	0.001
C7—C8	1.400 (0.001)	1.401 (0.001)	-0.001
C8—C9	1.398 (0.001)	1.397 (0.001)	0.001
C9—C3	1.409 (0.001)	1.408 (0.000)	0.001
C4—C10	1.409 (0.001)	1.407 (0.001)	0.002
C10—C11	1.398 (0.001)	1.399 (0.001)	-0.001
C11—C12	1.400 (0.001)	1.400 (0.001)	0.000
C12—C13	1.401 (0.001)	1.401 (0.001)	0.000
C13—C14	1.397 (0.001)	1.397 (0.001)	0.000
C14—C4	1.410 (0.001)	1.408 (0.000)	0.002
C3—C5—C6	120.9 (-0.600)	120.7 (0.00)	/
C1—C3—C5	122.2 (2.80)	119.8 (-0.1)	/
C2—C1—C3	124.9 (0.10)	126.2 (0.20)	/
C2—C1—C3—C5	25.5 (-2.90)	43.6 (0.2)	/
C4—C2—C1—C3	179.3 (0.10)	5.4 (-0.1)	/

TABLE S24. Optimized key geometrical parameters [bond lengths (Å), bond angles (°)] for *trans*- and *cis*-stilbene calculated at the SMD(benzene)//MP2/6-311G(d) level. The values in parenthesis are the differences between the geometrical parameter in benzene and the ones in gas phase.

	trans	*cis*	bond length difference, Δ = d(*t*) -d(*c*)
C1—C2	1.354 (0.000)	1.353 (0.000)	0.001
C2—C4	1.468 (0.000)	1.476 (0.000)	-0.008
C1—C3	1.468 (0.000)	1.476 (0.000)	-0.008
C3—C5	1.409 (0.000)	1.407 (0.001)	0.002
C5—C6	1.397 (0.001)	1.398 (0.000)	-0.002
C6—C7	1.400 (0.000)	1.399 (0.000)	0.001
C7—C8	1.399 (0.000)	1.401 (0.001)	-0.002
C8—C9	1.397 (0.000)	1.397 (0.001)	0.000
C9—C3	1.409 (0.001)	1.408 (0.000)	0.001
C4—C10	1.409 (0.001)	1.407 (0.001)	0.002
C10—C11	1.397 (0.000)	1.398 (0.000)	-0.001
C11—C12	1.399 (0.000)	1.399 (0.000)	0.000
C12—C13	1.400 (0.000)	1.401 (0.001)	-0.001
C13—C14	1.397 (0.001)	1.397 (0.001)	0.000
C14—C4	1.409 (0.000)	1.408 (0.000)	0.001
C3—C5—C6	120.9 (-0.600)	120.7 (0.00)	/
C1—C3—C5	122.3 (2.70)	119.8 (-0.1)	/
C2—C1—C3	124.9 (0.10)	126.3 (0.10)	/
C2—C1—C3—C5	26.6 (-1.80)	43.3 (-0.1)	/
C4—C2—C1—C3	179.2 (0.00)	5.4 (-0.1)	/

7.2. Second hyperpolarizabilities

Eq. (14) was widely-used to study the frequency dispersion of the $\gamma_{//}$ and $\gamma_{\perp}$ tensors.[28,30–36] Here, in addition to these quantities (Tables S26-S31 or FIGS. 8&9 and S4&S5), it was also applied to γ_{THS} whose expression is given by Eq. (S6). To do so, the rotational average $\langle\gamma^2_{ZZZZ}\rangle$ and $\langle\gamma^2_{ZXXX}\rangle$ quantities [Eqs. (S7) and (S8)] were estimated from the frequency-dependent dc-Kerr $[\gamma_{ijkl}(-\omega;\omega,0,0)]$ and EFISHG $[\gamma_{ijkl}(-2\omega;\omega,\omega,0)]$ second hyperpolarizability tensor components. Then, the dynamic γ_{THS} was estimated (Table S32) and expressed as a power series in ω_L^2 [FIG. S6].

TABLE S25: Static second hyperpolarizability (10^3 a.u.) and DR values as calculated at the SMD//CAM-B3LYP/6-311+G(d) level for *trans* and *cis* isomers, using the static ($\boldsymbol{\epsilon_0}$) and the optical ($\boldsymbol{\epsilon_\infty}$) relative dielectric constants for each solvent. *In vacuo* values are provided for comparison.

Medium	$\boldsymbol{\epsilon_0}$					$\boldsymbol{\epsilon_\infty}$		
	$\boldsymbol{\epsilon_0}$	$\boldsymbol{\epsilon_\infty}$	$\boldsymbol{\gamma_{//}}$	$\boldsymbol{\gamma_{THS}}$	DR_{THS}	$\boldsymbol{\gamma_{//}}$	$\boldsymbol{\gamma_{THS}}$	DR_{THS}
					***trans*-stilbene**			
in vacuo	1.000	1.000	109.1	162.7	9.1	109.1	162.7	9.1
Benzene	2.271	2.253	188.0	290.8	8.4	187.2	290.0	8.4
Chloroform	4.711	2.091	252.6	393.7	8.3	183.9	284.9	8.4
THF	7.426	1.974	283.6	442.0	8.3	179.9	278.6	8.4
1,2-DCE	10.125	2.087	301.1	469.1	8.3	186.5	289.5	8.4
					***cis*-stilbene**			
in vacuo	1.000	1.000	49.9	55.1	31.5	49.9	55.1	31.5
Benzene	2.271	2.253	79.9	89.8	27.0	79.6	89.4	27.0
Chloroform	4.711	2.091	106.5	119.5	26.5	76.7	86.1	27.0
THF	7.426	1.974	120.1	134.3	27.1	74.3	83.3	27.1
1,2-DCE	10.125	2.087	128.0	142.9	27.3	76.5	85.8	27.0

TABLE S26. Gas phase dc-Kerr and EFISHG second hyperpolarizabilities ($\gamma_{//}$) as a of function of the frequency ω (and of ω_L^2). The calculations were performed at the CAM-B3LYP/6-311+G(d) level using the superfine integration grid.

$\boldsymbol{\omega}$ **(a.u.)**	$\boldsymbol{\omega_L^2}$ $\boldsymbol{(eV^2)}$	$\boldsymbol{\gamma_{//}(-\omega;\ \omega,0,0)}$ **(a.u.)**	$\boldsymbol{\omega_L^2}$ $\boldsymbol{(eV^2)}$	$\boldsymbol{\gamma_{//}(-2\ \omega;\ \omega,\omega,0)}$ **(a.u.)**
		***trans*-stilbene**		
0.00	0.00	109151	0.00	109151
0.01	0.15	109935	0.44	111535
0.02	0.58	112347	1.75	119230
0.03	1.31	116566	3.94	134199
0.04	2.33	122934	7.00	161172
0.05	3.65	132006	10.94	212133
0.06	5.25	144684	15.75	325103
0.07	7.14	162441	21.43	703334
0.08	9.33	187758	27.99	-13284100
0.09	11.81	225057	35.43	-597571
0.10	14.58	282825	43.74	-735514
		***cis*-stilbene**		
0.00	0.00	49936	0.00	49936
0.01	0.15	50177	0.44	50666
0.02	0.58	50913	1.75	52979
0.03	1.31	52184	3.94	57316
0.04	2.33	54070	7.00	64685
0.05	3.65	56695	10.94	77413
0.06	5.25	60253	15.75	101922
0.07	7.14	65043	21.43	164512
0.08	9.33	71560	27.99	697666
0.09	11.81	80623	35.43	-98741
0.10	14.58	93708	43.74	14854

TABLE S27. dc-Kerr and EFISHG second hyperpolarizabilities ($\gamma_{//}$) as a function of the frequency ω (and of ω_L^2). The calculations were performed at the SMD (1,2-dichloroethane)//CAM-B3LYP/6-311+G(d) level using the superfine integration grid.

$\boldsymbol{\omega}$ **(a.u.)**	$\boldsymbol{\omega_L^2}$ $\boldsymbol{(eV^2)}$	$\boldsymbol{\gamma_{//}(-\omega;\ \omega,0,0)}$ **(a.u.)**	$\boldsymbol{\omega_L^2}$ $\boldsymbol{(eV^2)}$	$\boldsymbol{\gamma_{//}(-2\ \omega;\ \omega,\omega,0)}$ **(a.u.)**
		***trans*-stilbene**		
0.00	0.00	186514	0.00	186514
0.01	0.15	188060	0.44	191222
0.02	0.58	192826	1.75	206548
0.03	1.31	201219	3.94	236966
0.04	2.33	213997	7.00	293750
0.05	3.65	232447	10.94	407948
0.06	5.25	258698	15.75	695291
0.07	7.14	296344	21.43	2158200
0.08	9.33	351731	27.99	-2767400
0.09	11.81	436843	35.43	373837
0.10	14.58	576556	43.74	-1130790
		***cis*-stilbene**		
0.00	0.00	76492	0.00	76492
0.01	0.15	76904	0.44	77745
0.02	0.58	78170	1.75	81736
0.03	1.31	80361	3.94	89303
0.04	2.33	83628	7.00	102385
0.05	3.65	88212	10.94	125613
0.06	5.25	94475	15.75	172437
0.07	7.14	103015	21.43	303977
0.08	9.33	114808	27.99	2938510
0.09	11.81	131513	35.43	-30245
0.10	14.58	156206	43.74	141165

TABLE S28. dc-Kerr and EFISHG second hyperpolarizabilities ($\gamma_{//}$) as a function of the frequency ω (and of ω_L^2). The calculations were performed at the SMD(Tetrahydrofuran)//CAM-B3LYP/6-311+G(d) level using the superfine integration grid.

$\boldsymbol{\omega}$ **(a.u.)**	$\boldsymbol{\omega_L^2}$ $\boldsymbol{(eV^2)}$	$\boldsymbol{\gamma_{//}(-\omega;\ \omega, 0, 0)}$ **(a.u.)**	$\boldsymbol{\omega_L^2}$ $\boldsymbol{(eV^2)}$	$\boldsymbol{\gamma_{//}(-2\ \omega;\ \omega, \omega, 0)}$ **(a.u.)**
		***trans*-stilbene**		
0.00	0.00	179854	0.00	179854
0.01	0.15	181332	0.44	184352
0.02	0.58	185884	1.75	198983
0.03	1.31	193896	3.94	227976
0.04	2.33	206084	7.00	281952
0.05	3.65	223671	10.94	389965
0.06	5.25	248656	15.75	658824
0.07	7.14	284421	21.43	1969360
0.08	9.33	336912	27.99	-2857390
0.09	11.81	417309	35.43	100971
0.10	14.58	548647	43.74	-1109140
		***cis*-stilbene**		
0.00	0.00	74290	0.00	74290
0.01	0.15	74688	0.44	75498
0.02	0.58	75909	1.75	79345
0.03	1.31	78020	3.94	86634
0.04	2.33	81171	7.00	99221
0.05	3.65	85582	10.94	121528
0.06	5.25	91617	15.75	166356
0.07	7.14	99829	21.43	291437
0.08	9.33	111157	27.99	2577070
0.09	11.81	127190	35.43	-46934
0.10	14.58	150858	43.74	122321

TABLE S29. dc-Kerr and EFISHG second hyperpolarizabilities ($\gamma_{//}$) as a function of the frequency ω (and of ω_L^2). The calculations were performed at the SMD (Chloroform)//CAM-B3LYP/6-311+G(d) level using the superfine integration grid.

$\boldsymbol{\omega}$ **(a.u.)**	$\boldsymbol{\omega_L^2}$ $\boldsymbol{(eV^2)}$	$\boldsymbol{\gamma_{//}(-\omega;\ \omega,0,0)}$ **(a.u.)**	$\boldsymbol{\omega_L^2}$ $\boldsymbol{(eV^2)}$	$\boldsymbol{\gamma_{//}(-2\ \omega;\ \omega,\omega,0)}$ **(a.u.)**
		***trans*-stilbene**		
0.00	0.00	183937	0.00	183937
0.01	0.15	185453	0.44	188550
0.02	0.58	190120	1.75	203552
0.03	1.31	198333	3.94	233289
0.04	2.33	210837	7.00	288672
0.05	3.65	228872	10.94	399559
0.06	5.25	254505	15.75	675781
0.07	7.14	291208	21.43	2023880
0.08	9.33	345088	27.99	-2939800
0.09	11.81	427645	35.43	-84292
0.10	14.58	562576	43.74	-1154370
		***cis*-stilbene**		
0.00	0.00	76670	0.00	76670
0.01	0.15	77088	0.44	77930
0.02	0.58	78353	1.75	81936
0.03	1.31	80556	3.94	89535
0.04	2.33	83839	7.00	102676
0.05	3.65	88438	10.94	126018
0.06	5.25	94729	15.75	173107
0.07	7.14	103312	21.43	305606
0.08	9.33	115157	27.99	3024220
0.09	11.81	131948	35.43	-526555
0.10	14.58	156779	43.74	135869

TABLE S30. dc-Kerr and EFISHG second hyperpolarizabilities ($\gamma_{//}$) as a function of the frequency ω (and of ω_L^2). The calculations were performed at the SMD (Benzene)//CAM-B3LYP/6-311+G(d) level using the superfine integration grid.

$\boldsymbol{\omega}$ **(a.u.)**	$\boldsymbol{\omega_L^2}$ $\boldsymbol{(eV^2)}$	$\boldsymbol{\gamma_{//}(-\omega;\ \omega, 0, 0)}$ **(a.u.)**	$\boldsymbol{\omega_L^2}$ $\boldsymbol{(eV^2)}$	$\boldsymbol{\gamma_{//}(-2\ \omega;\ \omega, \omega, 0)}$ **(a.u.)**
		***trans*-stilbene**		
0.00	0.00	187226	0.00	187226
0.01	0.15	188761	0.44	191909
0.02	0.58	193504	1.75	207147
0.03	1.31	201849	3.94	237335
0.04	2.33	214542	7.00	293497
0.05	3.65	232854	10.94	405688
0.06	5.25	258863	15.75	683602
0.07	7.14	296073	21.43	2006940
0.08	9.33	350648	27.99	-3167350
0.09	11.81	434137	35.43	-433310
0.10	14.58	570286	43.74	-1220950
		***cis*-stilbene**		
0.00	0.00	79609	0.00	79609
0.01	0.15	80042	0.44	80928
0.02	0.58	81372	1.75	85127
0.03	1.31	83680	3.94	93096
0.04	2.33	87120	7.00	106897
0.05	3.65	91945	10.94	131469
0.06	5.25	98552	15.75	181243
0.07	7.14	107564	21.43	322702
0.08	9.33	120025	27.99	3808980
0.09	11.81	137713	35.43	-46205
0.10	14.58	163926	43.74	157867

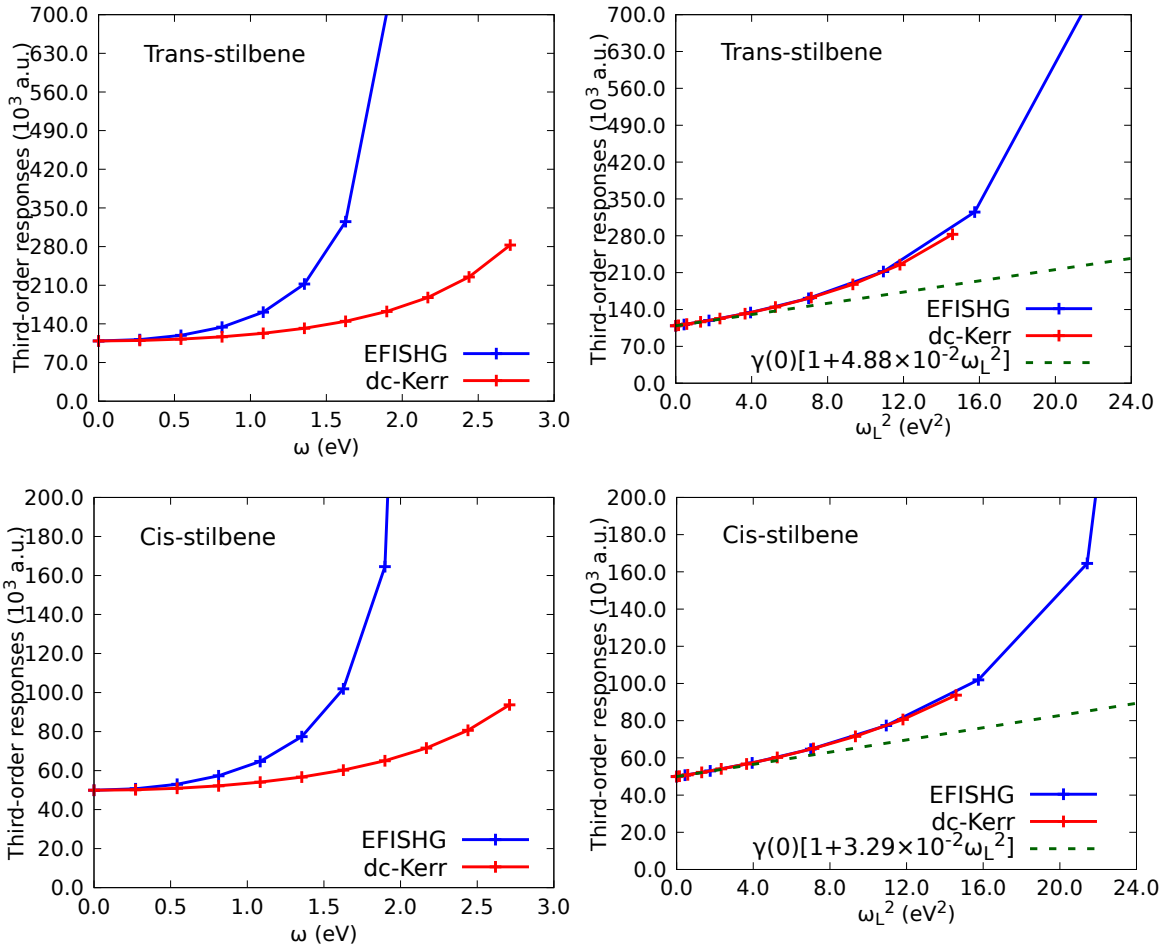

FIG S4. Gas phase TDDFT/CAM-B3LYP/6-311+G(d) dc-Kerr and EFISHG second hyperpolarizabilities ($\gamma_{//}$) as a function of the frequency (left) and ω_L^2 (right) for *trans*-stilbene and *cis*-stilbene.

TABLE S31. dc-Kerr and EFISHG second hyperpolarizabilities ($\gamma_\perp$) as a function of the frequency ω (and of ω_L^2). The calculations were performed at the SMD (1,2-DCE)//CAM-B3LYP/6-311+G(d) level using the superfine integration grid.

ω (a.u.)	ω_L^2 (eV^2)	$\gamma_\perp(-\omega;\ \omega,0,0)$ (a.u.)	ω_L^2 (eV^2)	$\gamma_\perp(-2\,\omega;\ \omega,\omega,0)$ (a.u.)
		***trans*-stilbene**		
0.00	0.00	62172	0.00	62172
0.01	0.15	62698	0.44	63748
0.02	0.58	64322	1.75	68880
0.03	1.31	67184	3.94	79069
0.04	2.33	71544	7.00	98099
0.05	3.65	77845	10.94	136387
0.06	5.25	86823	15.75	232759
0.07	7.14	99718	21.43	723285
0.08	9.33	118719	27.99	-926057
0.09	11.81	147964	35.43	213835
0.10	14.58	196057	43.74	-398071

$$\gamma_\perp(-\omega_\sigma;\ \omega_1,\omega_2,\omega_3) = 62.2 \times [1 + (5.90 \pm 0.01) \times 10^{-2} \times \omega_L^2(\mathrm{eV}^2) + \cdots] \qquad \text{(S18)}$$

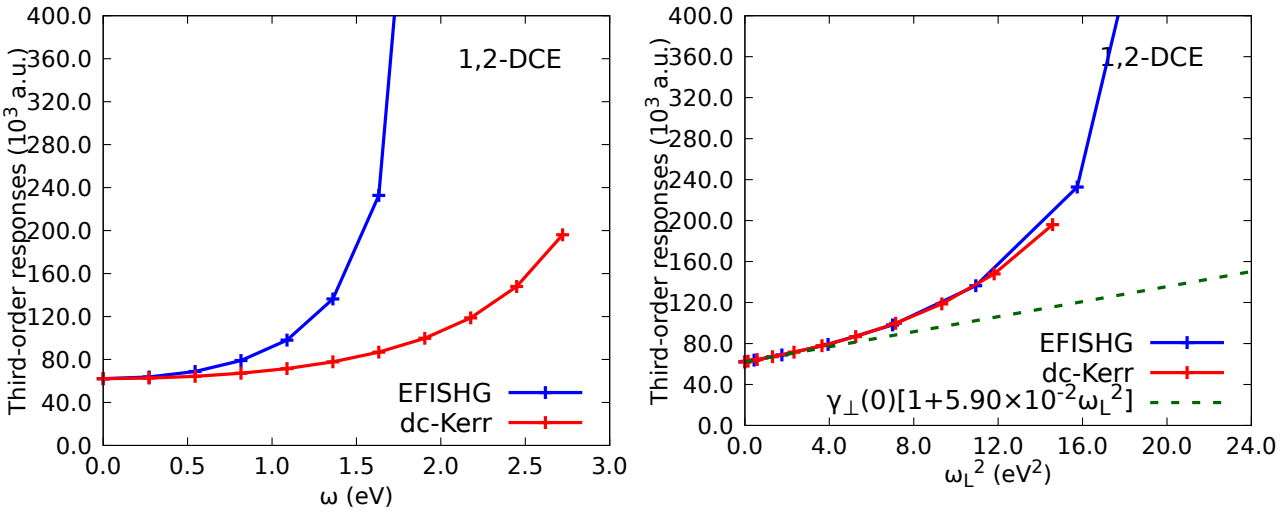

FIG S5. TDDFT/CAM-B3LYP/6-311+G(d) dc-Kerr and EFISHG second hyperpolarizabilities ($\gamma_\perp$) as a function of the frequency (left) and ω_L^2 (right) for *trans*-stilbene in 1,2-DCE solvent medium.

TABLE S32. THS responses (a.u.) as obtained from the dynamic dc-Kerr and EFISHG second hyperpolarizability tensor components as a function of the frequency ω (and of ω_L^2). The calculations were performed at the SMD (chloroform)//CAM-B3LYP/6-311+G(d) level using the superfine integration grid.

ω (a.u.)	ω_L^2 (eV^2)	γ_{THS} from $\gamma_{ijkl}(-\omega;\omega,0,0)$	ω_L^2 (eV^2)	γ_{THS} from $\gamma_{ijkl}(-2\,\omega;\,\omega,\omega,0)$
		***trans*-stilbene**		
0.00	0.00	284932	0.00	284932
0.01	0.15	287493	0.44	292713
0.02	0.58	295383	1.75	318086
0.03	1.31	309291	3.94	368625
0.04	2.33	330515	7.00	463424
0.05	3.65	361230	10.94	654957
0.06	5.25	405057	15.75	1137106
0.07	7.14	468095	21.43	3516412
0.08	9.33	561096	27.99	5325607
0.09	11.81	704354	35.43	2055419
0.10	14.58	939765	43.74	2239906

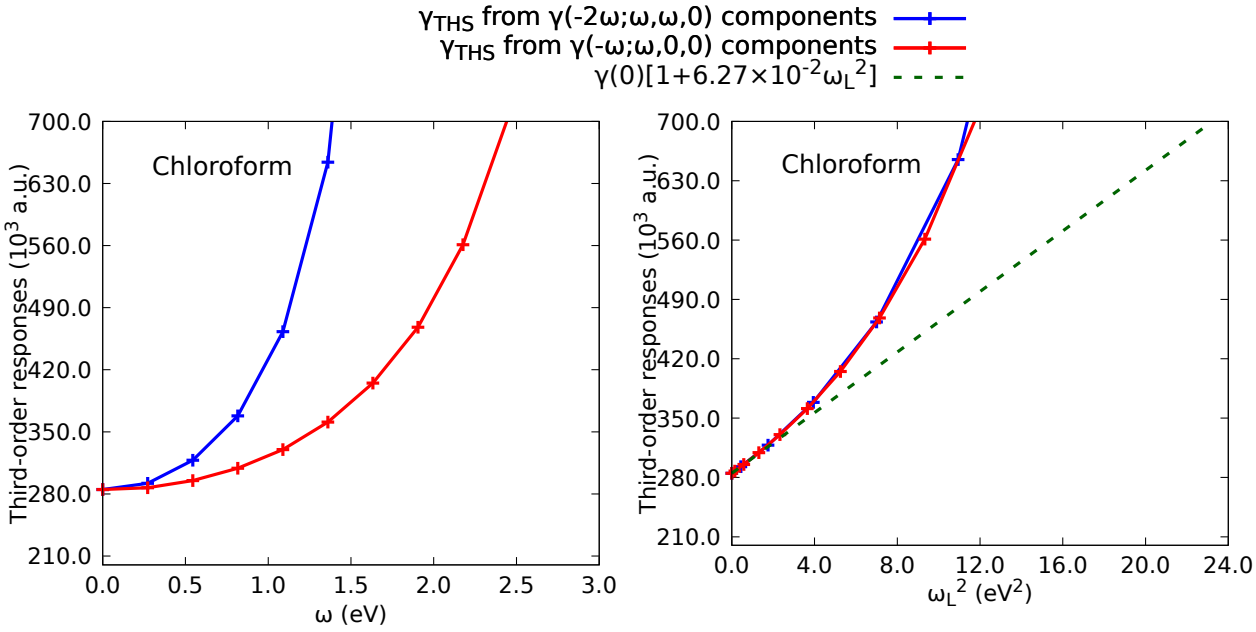

FIG S6. TDDFT/CAM-B3LYP/6-311+G(d) dc-Kerr and EFISHG second hyperpolarizabilities (γ_{THS}) as a function of the frequency (left) and ω_L^2 (right) for *trans*-stilbene in chloroform solvent medium. The superposition of the dc-Kerr and EFISHG curves on the right-hand side figure demonstrates that the the Bishop-like polynomial expressions can also be applied to γ_{THS}.

$$\gamma_{THS}(-\omega_\sigma;\,\omega_1,\omega_2,\omega_3) = 284.9\times10^3\times[1+(6.27\pm0.02)\times10^{-2}\times\omega_L^2(\mathrm{eV}^2)+\cdots] \quad \text{(S19)}$$

7.3. Theoretical and computational aspects on the vibrational second hyperpolarizabilities

When invoking the clamped nucleus (CN) approximation,[S39] adopting Bishop and Kirtman perturbation theory method,[S40,41] and employing the double (electrical and mechanical) harmonic approximation (the zero-point vibrational average contribution is therefore neglected), the vibrational second hyperpolarizability reads

$$\gamma^{vib} = [\alpha^2]^0 + [\mu\beta]^0 \tag{S20}$$

where the tensor components of both quantities are:

$$[\alpha^2]^0_{ijkl} = \frac{1}{8}\sum \mathrm{P}_{-\sigma,1,2,3} \sum_{\mathrm{a}} \frac{\left(\frac{\partial \alpha_{ij}}{\partial \mathrm{Q_a}}\right)_0 \left(\frac{\partial \alpha_{kl}}{\partial \mathrm{Q_a}}\right)_0}{\omega_{\mathrm{a}}^2 - (\omega_2^2 + \omega_3^2)} \tag{S21}$$

$$[\mu\beta]^0_{ijkl} = \frac{1}{6}\sum \mathrm{P}_{-\sigma,1,2,3} \sum_{\mathrm{a}} \frac{\left(\frac{\partial \mu_{i}}{\partial \mathrm{Q_a}}\right)_0 \left(\frac{\partial \beta_{jkl}}{\partial \mathrm{Q_a}}\right)_0}{(\omega_{\mathrm{a}}^2 - \omega_\sigma^2)} \tag{S22}$$

$\mathrm{P}_{-\sigma,1,2,3}$ is a summation over the 24 permutations of the pairs (ω_σ, i), (ω_1, j), (ω_2, k) and (ω_3, l), $\mathrm{Q_a}$ is the normal coordinate of the vibrational mode having circular frequency ω_{a} (the a index runs over all the 3N-6 vibrational normal coordinates), the subscript 0 indicates that the derivatives are evaluated at nuclear configuration equilibrium, and the subscripts $i, j, k\ldots$ stand for the Cartesian molecular axes x, y, z. Then, by applying the infinite optical frequency approximation,[S42,43] the dynamic vibrational second hyperpolarizabilities become frequency-independent and they can be written as simple multiple of their static counterparts:

$$\gamma^{vib}(-\omega;\ \omega, -\omega, \omega) = \frac{2}{3}[\alpha^2]^0_{\omega=0} \tag{S23}$$

$$\gamma^{vib}(-2\omega;\ \omega, \omega, 0) = \frac{1}{4}[\mu\beta]^0_{\omega=0} \tag{S24}$$

$$\gamma^{vib}(-3\omega;\ \omega, \omega, \omega) = 0 \tag{S25}$$

In this work, the geometrical derivatives of the static polarizability/first hyperpolarizability with respect to the atomic Cartesian coordinates were calculated by employing the finite distortion method in combination with Romberg's quadrature (distortion amplitude = 0.01 and 0.002 a.u. and one Romberg's iteration). In order to obtain the derivatives with respect to the vibrational normal mode coordinates, the derivatives with respect to the atomic Cartesian coordinates were projected over the normal coordinates. The Hessian required to compute the vibrational normal modes and frequencies were calculated analytically at the DFT level by using the coupled-perturbed Kohn–Sham (CPKS) scheme. The static polarizability/first hyperpolarizability calculations were performed with the CPKS//CAM-B3LYP XC functional. Solvent (1,2-dichloroethane, chloroform and tetrahydrofuran) effects were included by using IEFPCM.

7.4. Linear optical properties

TABLE S33. Vertical absorption wavelength (λ_{01}, nm), excitation energy (ΔE_{01}, eV), and oscillator strength (f_{01}, dimensionless) of the dominant lowest-energy state of *trans*-stilbene as computed at the TDDFT//CAM-B3LYP/6-311+G(d) level *in vacuo* and in different solvents. The values in parentheses in the third and fourth column corresponds to the experimental maximum absorption values. These demonstrate very small solvatochromic effects. Note that the maximum absorption band in benzene corresponds to the so-called 0-1 vibronic transition whereas it is the 0-2 one in chloroform and in ethanol.

	Transition [character (%)]	$\boldsymbol{\lambda_{01}}$	$\boldsymbol{\Delta E_{01}}$	$\boldsymbol{f_{01}}$
In vacuo	$S_0 \rightarrow S_1$ [H→L (0.96)]	286	4.32	0.870
Benzene	$S_0 \rightarrow S_1$ [H→L (0.97)]	301 (311[S37])	4.12 (3.99)	1.060
Chloroform	$S_0 \rightarrow S_1$ [H→L (0.97)]	309 (298[S37])	4.02 (4.16)	1.159
THF	$S_0 \rightarrow S_1$ [H→L (0.97)]	312	3.97	1.196
1,2-DCE	$S_0 \rightarrow S_1$ [H→L (0.97)]	314 (298[S38])	3.95 (4.16)	1.216
Ethanol (95%)		(295 [S38])	(4.20)	

TABLE S34. Vertical absorption wavelengths (λ_{0i}, nm), excitation energies (ΔE_{0i}, eV), and oscillator strengths (f_{0i}, dimensionless) of the two dominant lowest-energy states of the *cis*-stilbene as computed at the TDDFT//CAM-B3LYP/6-311+G(d) level *in vacuo* and different solvents. The last line reports experimental values of the absorption maximum, for comparison purpose.

	Transistion [character (%)]	λ_{0i}	ΔE_{0i}	f_{0i}
In vacuo	$S_0 \rightarrow S_1$ [H→L (0.96)]	276	4.49	0.316
	$S_0 \rightarrow S_5$ [H-1→L (0.50)]	216	5.74	0.310
Benzene	$S_0 \rightarrow S_1$ [H→L (0.96)]	282	4.40	0.439
	$S_0 \rightarrow S_5$ [H-1→L (0.54)]	219	5.66	0.506
Chloroform	$S_0 \rightarrow S_1$ [H→L (0.96)]	285	4.35	0.512
	$S_0 \rightarrow S_5$ [H-1→L (0.57)]	222	5.60	0.644
THF	$S_0 \rightarrow S_1$ [H→L (0.97)]	28	4.33	0.541
	$S_0 \rightarrow S_5$ [H-1→L (0.57)]	223	5.57	0.709
1,2-DCE	$S_0 \rightarrow S_1$ [H→L (0.96)]	287	4.32	0.558
	$S_0 \rightarrow S_5$ [H-1→L (0.57)]	223	5.55	0.743
ethanol		280 [S38]	4.43	
		224 [S38]	5.54	

References

S1 S. Ghosal, M. Samoc, P. N. Prasad and J. J. Tufariello, Optical nonlinearities of organometallic structures: aryl and vinyl derivatives of ferrocene, *J. Phys. Chem.*, 1990, **94**, 2847–2851.

S2 D. V Vlasov, R. A. Garaev, V. V Korobkin and R. V Serov, Measurement of nonlinear polarizability of air, 1979, **2045**, 1033–1036.

S3 Y. Shimoji, A. T. Fay, R. S. F. Chang and N. Djeu, Direct measurement of the nonlinear refractive index of air, *J. Opt. Soc. Am. B*, 1989, **6**, 1994.

S4 D. M. Pennington, M. A. Henesian and R. W. Hellwarth, Nonlinear index of air at 1.053 μm, *Phys. Rev. A*, 1989, **39**, 3003–3009.

S5 J. L. Brédas, C. Adant, P. Tackx, A. Persoons and B. M. Pierce, Third-Order Nonlinear Optical Response in Organic Materials: Theoretical and Experimental Aspects, *Chem. Rev.*, 1994, **94**, 243–278.

S6 P. Tackx, M. Kauranen and A. Persoons, Determination of resonant and nonresonant third-order nonlinearities of organic molecules by phase-conjugate interferometry, *Opt. Lett.*, 1994, **19**, 1113.

S7 D. M. Bishop, Molecular vibrational and rotational motion in static and dynamic electric fields, *Rev. Mod. Phys.*, 1990, **62**, 343–374.

S8 L. L. Boyle, A. D. Buckingham, R. L. Disch and D. A. Dromor, Higher polarizability of the helium atom, *J. Chem. Phys.*, 1966, **45**, 1318–1323.

S9 R. Tammer, K. Löblein, K. H. Peting and W. Hüttner, Field calibrated measurements of the dc Kerr constants of helium and molecular hydrogen, *Chem. Phys.*, 1992, **168**, 151–158.

S10 D. P. Shelton and B. Rugar, The Kerr effect in hydrogen, *Chem. Phys. Lett.*, 1993, **201**, 364–368.

S11 D. P. Shelton and J. E. Rice, Measurements and Calculations of the Hyperpolarizabilities of Atoms and Small Molecules in the Gas Phase, *Chem. Rev.*, 1994, **94**, 3–29.

12 R. Tammer and W. Hüttner, The anisotropy of the second hyperpolarizability of molecular hydrogen from the pressure and temperature dependence of the Kerr effect, *Chem. Phys.*, 1990, **146**, 155–163.

S13 D. M. Bishop, 1998, pp. 1–40.

S14 D. P. Shelton and J. E. Rice, Measurements and calculations of the hyperpolarizabilities of atoms and small molecules in the gas phase, *Chem. Rev.*, 1994, **94**, 3–29.

S15 N. Van Steerteghem, K. Clays, T. Verbiest and S. Van Cleuvenbergen, Third-Harmonic Scattering for Fast and Sensitive Screening of the Second Hyperpolarizability in Solution, *Anal. Chem.*, 2017, **89**, 2964–2971.

S16 V. Rodriguez, Polarization-Resolved Third-Harmonic Scattering in Liquids, *J. Phys. Chem. C*, 2017, **121**, 8510–8514.

S17 D. L. Andrews and T. Thirunamachandran, On three-dimensional rotational averages, *J. Chem. Phys.*, 1977, **67**, 5026–5033.

S18 J. S. Ford and D. L. Andrews, Molecular Tensor Analysis of Third-Harmonic Scattering in Liquids, *J. Phys. Chem. A*, 2018, **122**, 563–573.

S19 P. Beaujean and B. Champagne, Coupled cluster evaluation of the second and third harmonic scattering responses of small molecules, *Theor. Chem. Acc.*, 2018, **137**, 50.

S20 J. Autschbach and M. Srebro, Delocalization error and ‘functional tuning’ in Kohn-Sham calculations of molecular properties, *Acc. Chem. Res.*, 2014, **47**, 2592–2602.

S21 E. R. Johnson, A. Otero-de-la-Roza and S. G. Dale, Extreme density-driven delocalization error for a model solvated-electron system, *J. Chem. Phys.*, 2013, **139**, 184116.

S22 E. R. Johnson, P. Mori-Sánchez, A. J. Cohen and W. Yang, Delocalization errors in density functionals and implications for main-group thermochemistry, *J. Chem. Phys.*, 2008, **129**, 204112.

S23 T. J. Duignan, J. Autschbach, E. Batista and P. Yang, Assessment of Tuned Range Separated

Exchange Functionals for Spectroscopies and Properties of Uranium Complexes, *J. Chem. Theory Comput.*, 2017, **13**, 3614–3625.
S24 A. K. Pal, T. J. Duignan and J. Autschbach, Calculation of linear and nonlinear optical properties of azobenzene derivatives with Kohn-Sham and coupled-cluster methods, *Phys. Chem. Chem. Phys.*, 2018, **20**, 7303–7316.
S25 S. Nénon, B. Champagne and M. I. Spassova, Assessing long-range corrected functionals with physically-adjusted range-separated parameters for calculating the polarizability and the second hyperpolarizability of polydiacetylene and polybutatriene chains, *Phys. Chem. Chem. Phys.*, 2014, **16**, 7083–7088.
S26 R. Zaleśny, M. Medved', S. P. Sitkiewicz, E. Matito and J. M. Luis, Can Density Functional Theory Be Trusted for High-Order Electric Properties? The Case of Hydrogen-Bonded Complexes, *J. Chem. Theory Comput.*, 2019, **15**, 3570–3579.
S27 K. Garrett, X. Sosa Vazquez, S. B. Egri, J. Wilmer, L. E. Johnson, B. H. Robinson and C. M. Isborn, Optimum exchange for calculation of excitation energies and hyperpolarizabilities of organic electro-optic chromophores, *J. Chem. Theory Comput.*, 2014, **10**, 3821–3831.
S28 K. S. Kaka, P. Beaujean, F. Castet and B. Champagne, A quantum chemical investigation of the second hyperpolarizability of p -nitroaniline, *J. Chem. Phys.*, 2023, **159**, 114104.
S29 P. Besalú-Sala, S. P. Sitkiewicz, P. Salvador, E. Matito and J. M. Luis, A new tuned range-separated density functional for the accurate calculation of second hyperpolarizabilities, *Phys. Chem. Chem. Phys.*, 2020, **22**, 11871–11880.
S30 D. P. Shelton, Hyperpolarizability dispersion measured for Kr and Xe, *J. Chem. Phys.*, 1985, **84**, 404–407.
S31 D. M. Bishop, Dispersion Formulas for Certain Nonlinear Optical Processes, *Phys. Rev. Lett.*, 1988, **61**, 322–324.
S32 D. M. Bishop, General dispersion formulae for atomic third-order non-linear optical properties, *Chem. Phys. Lett.*, 1988, **153**, 441–445.
S33 D. M. Bishop, General dispersion formulas for molecular third-order nonlinear optical properties, *J. Chem. Phys.*, 1989, **90**, 3192–3195.
S34 D. M. Bishop and D. W. De Kee, The frequency dependence of nonlinear optical processes, *J. Chem. Phys.*, 1996, **104**, 9876–9887.
S35 D. M. Bishop and D. W. De Kee, The frequency dependence of hyperpolarizabilities for noncentrosymmetric molecules, *J. Chem. Phys.*, 1996, **105**, 8247–8249.
S36 P. Beaujean and B. Champagne, Coupled cluster evaluation of the frequency dispersion of the first and second hyperpolarizabilities of water, methanol, and dimethyl ether, *J. Chem. Phys.*, 2016, **145**, 044311.
S37 H. Suzuki, Relations between Electronic Absorption Spectra and Spatial Configurations of Conjugated Systems. XI Styrene, 1,1-Diphenylethylene and their Methylated Derivatives, *Bull. Chem. Soc. Jpn.*, 1960, **33**, 379–388.
S38 A. P. Persoons, B. M. Van Wonterghem and P. C. Tackx, in *Nonlinear Optics II*, eds. R. A. Fisher and J. F. Reintjes, SPIE, 1991, vol. 1409, p. 220.
S39 D. M. Bishop, B. Kirtman and B. Champagne, Differences between the exact sum-over-states and the canonical approximation for the calculation of static and dynamic hyperpolarizabilities, *J. Chem. Phys.*, 1997, **107**, 5780–5787.
S40 D. M. Bishop and B. Kirtman, A perturbation method for calculating vibrational dynamic dipole polarizabilities and hyperpolarizabilities, *J. Chem. Phys.*, 1991, **95**, 2646–2658.
S41 D. M. Bishop and B. Kirtman, Compact formulas for vibrational dynamic dipole polarizabilities and hyperpolarizabilities, *J. Chem. Phys.*, 1992, **97**, 5255–5256.
S42 D. M. Bishop, M. Hasan and B. Kirtman, A simple method for determining approximate static and dynamic vibrational hyperpolarizabilities, *J. Chem. Phys.*, 1995, **103**, 4157–4159.
S43 D. S. Elliott and J. F. Ward, Vibrational mode contributions to molecular third order polarizabilities, *Mol. Phys.*, 1984, **51**, 45–63.